Journal of Structural Geology 106 (2018) 1–18

Contents lists available at ScienceDirect

Journal of Structural Geology

journal homepage: www.elsevier.com/locate/jsg

Activation of preexisting transverse structures in an evolving magmatic rift in East Africa

J.D. Muirhead[a,b,*], S.A. Kattenhorn[c,b]

[a] Department of Earth Sciences, Syracuse University, 204 Heroy Geology Laboratory, Syracuse, NY 13244, USA
[b] Department of Geological Sciences, University of Idaho, 875 Perimeter Drive, Moscow, ID 83844, USA
[c] Department of Geological Sciences, University of Alaska Anchorage, Anchorage, AK 99508, USA

ARTICLE INFO

Keywords:
Fault evolution
Continental rifting
Inherited crustal fabric
Magmatic rifting
Magadi basin
Kenya Rift

ABSTRACT

Inherited crustal weaknesses have long been recognized as important factors in strain localization and basin development in the East African Rift System (EARS). However, the timing and kinematics (e.g., sense of slip) of transverse (rift-oblique) faults that exploit these weaknesses are debated, and thus the roles of inherited weaknesses at different stages of rift basin evolution are often overlooked. The mechanics of transverse faulting were addressed through an analysis of the Kordjya fault of the Magadi basin (Kenya Rift). Fault kinematics were investigated from field and remote-sensing data collected on fault and joint systems. Our analysis indicates that the Kordjya fault consists of a complex system of predominantly NNE-striking, rift-parallel fault segments that collectively form a NNW-trending array of en echelon faults. The transverse Kordjya fault therefore reactivated existing rift-parallel faults in ~1 Ma lavas as oblique-normal faults with a component of sinistral shear. In all, these fault motions accommodate dip-slip on an underlying transverse structure that exploits the Aswa basement shear zone. This study shows that transverse faults may be activated through a complex interplay among magma-assisted strain localization, preexisting structures, and local stress rotations. Rather than forming during rift initiation, transverse structures can develop after the establishment of pervasive rift-parallel fault systems, and may exhibit dip-slip kinematics when activated from local stress rotations. The Kordjya fault is shown here to form a kinematic linkage that transfers strain to a newly developing center of concentrated magmatism and normal faulting. It is concluded that recently activated transverse faults not only reveal the effects of inherited basement weaknesses on fault development, but also provide important clues regarding developing magmatic and tectonic systems as young continental rift basins evolve.

1. Introduction

Inherited crustal weaknesses—such as steeply dipping foliation planes, fracture sets and shear zones—are known to play important roles in localizing strain and influencing the architecture of continental rifts (Dixon et al., 1987; Rosendahl, 1987; Daly et al., 1989; Dunbar and Sawyer, 1989; Hetzel and Strecker, 1994). At some rift settings, like the East African Rift System (EARS), far-field tectonic forces are theoretically too small to rupture the thick continental lithosphere (Buck, 2004; Buck, 2006; Stamps et al., 2014). Such rifts are thought to initiate in zones of intense magmatism (Kendall et al., 2005; Beutel et al., 2010; Bialas et al., 2010; Daniels et al., 2014; Mana et al., 2015), fluid-driven weakening (Hui et al., 2015; Leseane et al., 2015; Muirhead et al., 2016; Weinstein et al., 2017), and along preexisting lithospheric weaknesses (Keranen and Klemperer, 2008; Katumwehe et al., 2015a). Early-stage rift basins (< 10 Ma) provide ideal natural laboratories for investigating the effects of these processes on rift initiation and development (Modisi et al., 2000; Calais et al., 2008; Kinabo et al., 2008; Le Gall et al., 2008; Laó-Dávila et al., 2015; Muirhead et al., 2015, 2016; Lee et al., 2016).

The earliest stages of rifting involve a competition between the formation of new, optimally oriented faults in strong, intact rock, and non-optimally oriented faults that follow and exploit preexisting crustal weaknesses, and thus require lower differential stresses to activate (Youash, 1969; Sibson, 1985; Smith and Mosley, 1993; Morley, 1995; Morley et al., 2004; Agostini et al., 2009; Corti, 2012). Newly developed faults that define the dominant structural fabric of the rift system are expected to trend orthogonal to the regional least compressive stress (σ_3) (Anderson, 1951) and have been previously termed orthogonal faults (e.g., Morley et al., 2004). Here, they are referred to as *rift-parallel faults* to avoid mechanical inferences based purely on fault orientation. Faults trending oblique to the dominant rift trend (oblique to the

* Corresponding author. Department of Earth Sciences, Syracuse University, 204 Heroy Geology Laboratory, Syracuse, NY 13244, USA.
E-mail address: james.muirhead@fulbrightmail.org (J.D. Muirhead).

https://doi.org/10.1016/j.jsg.2017.11.004
Received 17 September 2017; Received in revised form 30 October 2017; Accepted 6 November 2017
Available online 10 November 2017
0191-8141/ © 2017 Elsevier Ltd. All rights reserved.

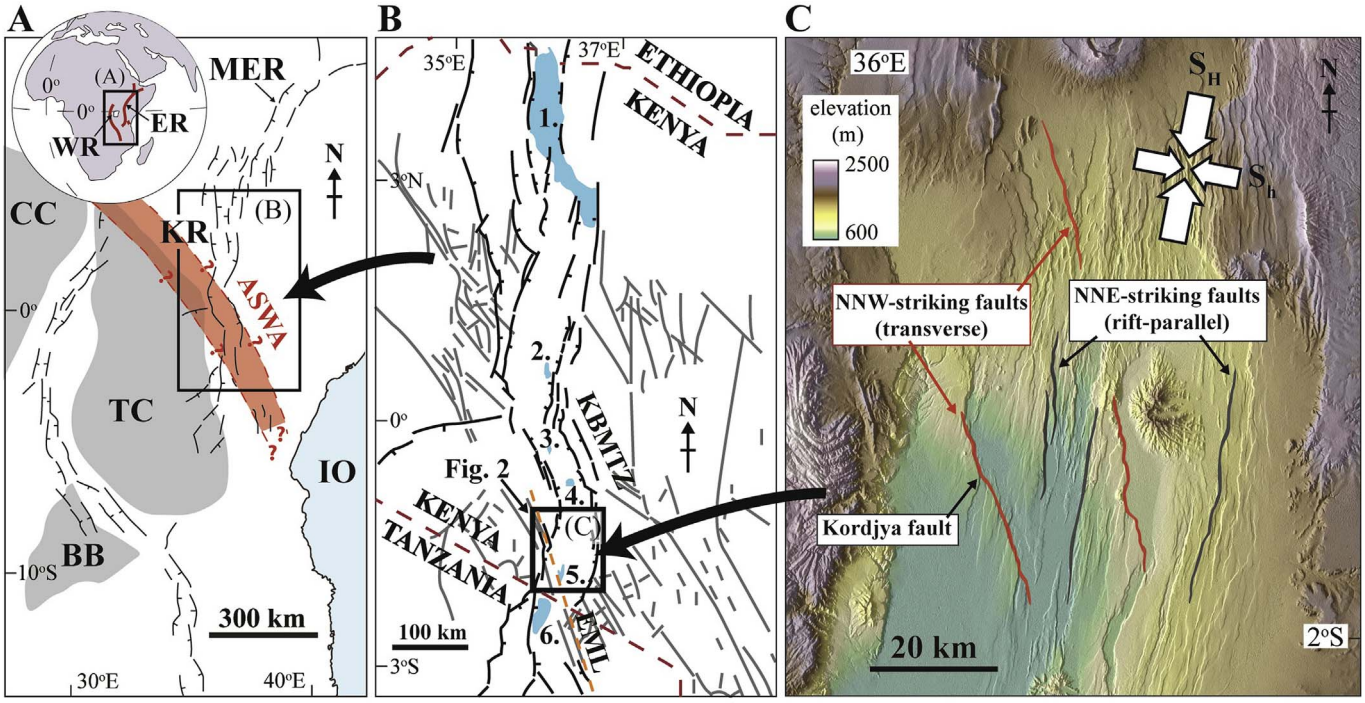

Fig. 1. A: Distribution of major rift faults (black lines) across East Africa. Grey polygons represent Archean cratons; white fill represents Proterozoic basement rocks (after Corti, 2009; Morley, 2010). Annotated are the Congo Craton (CC), Tanzanian Craton (TC), and Bangweulu Block (BB), as well as the Main Ethiopian Rift (MER), Kenya Rift (KR), and Indian Ocean (IO). The general location and trend of the Aswa shear zone (ASWA) is illustrated in red, with its distribution based on Smith (1994) and Katumwehe et al. (2015b). Inset (globe) shows the location of the map in A. Annotated on the globe are the Eastern rift branch (ER) and Western rift branch (WR) of the East African Rift System, shown as red lines. B: Distribution of major rift faults (black lines) and preexisting basement structures (grey lines) in the Kenya Rift (after Smith and Mosley, 1993). Also annotated are the Kerio-Bogoria-Marmanet transfer zone (KBMTZ) and major basin lakes, including (1) Turkana, (2) Baringo, (3) Nakuru, (4) Naivasha, (5) Magadi, and (6) Natron. The Engorika-Magadi-Lembolos (EML) lineament, along which the Kordjya fault lies, is shown as a dashed orange line. C: Annotated Shuttle Radar Topography Mission (SRTM) map of the Magadi basin. Selected examples of transverse (red) and rift-parallel (black) faults are annotated. The approximate orientations of the greatest (S_H) and least (S_h) horizontal compressive stress, based on data from Ibs-von Seht et al. (2001) and Atmaoui and Hollnack (2003), are illustrated by white arrows. Transverse faults trend oblique, whereas rift-parallel faults trend normal, to the regional least compressive stress prevalent throughout the basin. Note how transverse faults in C trend roughly parallel to the dominant NNW-SSE strike of the preexisting basement structures in B. (For interpretation of the references to colour in this figure legend, the reader is referred to the web version of this article.)

regional σ_3) often initiate along preexisting weaknesses that cut across the dominant fault fabric (Morley et al., 2004), and are referred to here as *transverse faults* (e.g., Ben-Avraham and Ten Brink, 1989) (Fig. 1C).

In the East African Rift System, the effects of preexisting weaknesses on the distribution and nature of faulting are visible on many scales (Morley, 1995) (Fig. 1). At the continental scale, rift basins preferentially form within Proterozoic basement rocks and are located near the margins of Archean cratons (e.g., Tanzanian craton) (Daly et al., 1989; Smith and Mosley, 1993; Ring, 1994; Simiyu and Keller, 2001; Morley, 2010) (Fig. 1A). This effect has divided the entire rift system into distinct Eastern and Western rifts (Rosendahl, 1987; Chorowicz, 1992; Koptev et al., 2015). Ductile and brittle shear zones in basement rocks also exhibit a control on rift basin segmentation and orientation. For example, a series of N to NW-trending basement shear zones, with lengths of up to thousands of km (e.g., Aswa shear zone; Chorowicz, 1989; Katumwehe et al., 2015b), have been documented throughout east and northeast Africa from field, remote-sensing, and geophysical studies (Smith and Mosley, 1993; Hetzel and Strecker, 1994; Birt et al., 1997; Vauchez et al., 2005; Katumwehe et al., 2015b; Robertson et al., 2015). These shear zones are responsible for abrupt changes in the orientation of the rift, such as the 130-km-long, NNW-trending Kerio-Bogoria-Marmanet transfer zone (Smith and Mosley, 1993), which accommodates an overall left step in the central Kenya Rift between Lake Baringo and Lake Naivasha (Chorowicz, 1989; Hetzel and Strecker, 1994; Le Turdu et al., 1999) across the trend of the Aswa shear zone (Fig. 1B). Preexisting basement shear zones also control the location of transfer zones between major rift-bounding faults (Chorowicz, 1989, 1992; Morley et al., 1990; Smith and Mosley, 1993; Ring, 1994). At still smaller scales, inherited weaknesses control the orientations and kinematics of shorter faults (lengths no greater than a few tens of kilometers) within the centers of rift basins (Le Turdu et al., 1999; Le Gall et al., 2000; Manighetti et al., 2001; Corti et al., 2007) (Fig. 1C).

Many questions exist regarding the state of stress (orientation of the minimum compressive stress, σ_3) and kinematics (e.g., sense of slip) of faulting during the reactivation of preexisting structures in the EARS. During rift initiation, when lithosphere is theoretically thicker and, hence, stronger (Buck, 2004), some fault systems may initiate on lithospheric weaknesses, often trending oblique to the regional extension direction and dominant NNE-SSW trend of the rift (Rosendahl, 1987; Versfelt and Rosendahl, 1989; Chorowicz, 1992; Chorowicz and Sorlien, 1992; Kilembe and Rosendahl, 1992; Modisi et al., 2000; Corti, 2008). Transverse faults exploiting these obliquely-oriented weaknesses are theoretically expected to fail as either oblique-normal or strike-slip faults (Rosendahl, 1987; Kilembe and Rosendahl, 1992; Le Turdu et al., 1999; Corti, 2008; Agostini et al., 2009).

Although field kinematic indicators often support this view (Chorowicz, 1989, 1992; Chorowicz and Sorlien, 1992; Ring et al., 1992; Wheeler and Karson, 1994), regional syntheses of recent focal mechanisms show that many transverse structures exhibit dip-slip (normal) kinematics (e.g., Koehn et al., 2010; Delvaux and Barth, 2010; Kolawole et al., 2017), which is also supported by field kinematic data collected on rift-bounding faults in the Main Ethiopian Rift (Agostini et al., 2011). Dip-slip faulting along transverse structures requires a rotation of σ_3 away from the *first-order* (regional) extension direction (~E-W to ESE-WNW) imposed by plate boundary forces across the EARS (Lithgow-Bertelloni and Guynn, 2004; Stamps et al., 2008; Saria et al., 2014). Such rotations could be produced by *second-order* stress fields, with length-scales on the order of 100–1000 km, resulting from

processes such as lithospheric flexure and buoyancy forces related to elevated mantle temperatures (Zoback, 1992). Alternatively, rotations may be related to *third-order* stress fields, typically occurring on scales of < 100 km along rift systems, and which drive stress perturbations locally within and between individual rift segments (Delvaux and Barth, 2010). In the EARS, these third-order stress fields are inferred to result from: (1) mechanical interactions between segmented rift basins (Koehn et al., 2008, 2010; Agostini et al., 2009; Muirhead et al., 2015); (2) strength anisotropies related to the presence of shear zones (Morley, 2010; Corti et al., 2013; Philippon et al., 2015); (3) volcano topography (Tibaldi et al., 2014); and (4) magma overpressures (Ring et al., 2005; Muirhead et al., 2015; Weinstein et al., 2017). Temporal variations in the regional stress state across the entire EARS, resulting from changes in far-field plate boundary forces, have also been inferred from the geological record (Strecker and Bosworth, 1991; Delvaux et al., 1992; Ring et al., 1992; Delvaux, 2001), although recent authors advocate that Nubia-Somalia plate motion has remained relatively stable for the last 10–12 Myr, with no significant variations in the extension direction across the EARS (Iaffaldano et al., 2014; DeMets and Merkouriev, 2016).

Together, these studies suggest that the role of preexisting weaknesses should vary over the course of rift evolution. For example, transverse structures should activate/deactivate in response to changes in far-field plate boundary forces, as well as more localized rotations of σ_3 as segmented basins progressively merge and interact, and new zones of focused magmatism develop (Morley et al., 1990; Schlische, 1993; Modisi et al., 2000; Densmore et al., 2007; Ebinger et al., 2013). Furthermore, long-term rifting should be accompanied by lithospheric strength reductions (due to heating and thinning) and the formation of new, optimally-oriented, rift-parallel faults; therefore, non-optimally oriented, transverse faults should be progressively abandoned as rift basins evolve (Chorowicz and Sorlien, 1992; Ebinger, 2005; Corti, 2008; Agostini et al., 2009). The Kenya Rift of the EARS exhibits numerous transverse faults that trend subparallel to NW-trending basement structures (Mosley, 1993; Smith and Mosley, 1993; Le Turdu et al., 1999; Robertson et al., 2015) (Fig. 1). Here, we test the timing and kinematics of transverse faulting through an analysis of the Kordjya fault of the Magadi basin, Kenya, and consider its role in accommodating the evolving rift basin segmentation in this part of the southern Kenya Rift.

2. Transverse faulting in the Magadi basin of the Kenya Rift

The Kenya Rift is a ~900-km-long sector of the EARS comprising a series of discrete, asymmetric rift basins, ~100 km long and tens of km wide (Foster et al., 1997; Acosta et al., 2015) (Fig. 1B). Faulting in the Kenya Rift initiated ~25 Ma near Lake Turkana (Morley et al., 1992; Ebinger et al., 2000, Fig. 1B). Since then, extension has gradually migrated southward along the Kenya Rift, with rift basins forming in central Kenya (e.g., Naivasha-Nakuru basin at 10–15 Ma; Smith, 1994; Spiegel et al., 2007; Acosta et al., 2015), and southern Kenya (e.g., the Magadi basin by 7 Ma; Crossley, 1979) (Fig. 1B). Upper crustal strain in the Kenya Rift is primarily accommodated along two types of fault systems: (1) *border faults*, which bound the rift and are hundreds of kilometers long and accrue thousands of meters of throw; and (2) *intra-rift faults*, which are smaller than border faults (tens of kilometers long, with tens to hundreds of meters of throw) and form in the central, inner depressions of rift basins (Corti, 2009; Muirhead et al., 2016).

The Magadi basin (Figs. 1C and 2) consists of volcanic and sedimentary sequences (23 Ma to present) that are pervasively faulted and overlie Mozambique Belt basement rocks (Baker, 1958, 1963; Baker and Mitchell, 1976; Crossley, 1979; Nyamai et al., 2003). It is bounded to the west by the ~7 Ma Nguruman border fault escarpment (Crossley, 1979; Birt et al., 1997; Muirhead et al., 2016). Pervasive intra-rift faults dissect < 3 Ma volcanics in the center of the basin (Baker, 1958; Baker and Mitchell, 1976; Atmaoui and Hollnack, 2003). Recent analysis of the distribution of fault strain within the Magadi basin (Muirhead et al., 2016) suggests that the locus of faulting has begun to migrate away from the border fault and into the center of the basin, within the intra-rift fault population. A number of transverse fault structures are observed within this intra-rift fault system. They are hypothesized to have formed during reactivation of NNW-trending basement fabrics (Smith and Mosley, 1993; Le Turdu et al., 1999) (Fig. 1B and C).

Previous studies investigating the development and kinematics of transverse faults in the Magadi basin also focused on the Kordjya fault (Le Turdu et al., 1999; Atmaoui and Hollnack, 2003) (Fig. 2). This fault bounds the western shore of Lake Magadi near the center of the basin. Towards the NW and away from the center of the rift basin, the Kordjya fault cuts obliquely across the dominant rift-parallel fault fabric and aligns along-strike with a subsidiary segment of the Nguruman border fault (Lengitoto segment; Fig. 2) at its northwestern end. Previous studies (e.g., Smith and Mosley, 1993; Le Turdu et al., 1999) proposed that the Kordjya fault follows a preexisting, basement shear zone (Aswa shear zone) that was reactivated either before or synchronously with the dominant, rift-parallel fault pattern in response to an ESE-WNW directed extension. Accordingly, earthquake focal mechanisms, analyses of neo-tectonic joints (~10 ka to present), and the dominant NNE-trending intra-rift fault pattern, all suggest that σ_3 is oriented ESE-WNW across the Magadi basin (Ibs-von Seht et al., 2001; Atmaoui and Hollnack, 2003) (Fig. 2). The assertion has been that the Kordjya fault, and similar NW-trending transverse faults in the Kenya Rift, formed as oblique-normal faults with a dextral component of shear (Smith and Mosley, 1993; Le Turdu et al., 1999; Atmaoui and Hollnack, 2003). If this were the case, ESE-WNW extension should impart roughly equal amounts of normal dip-slip and dextral strike-slip motion along the Kordjya fault.

Current hypotheses regarding the development of the Kordjya fault system are conceptually sound from a fault-mechanical and rift evolution perspective (e.g., Rosendahl, 1987; Chorowicz, 1989; Kilembe and Rosendahl, 1992). For example, analogue and numerical modeling of continental rifting in zones of inherited weaknesses oriented oblique to the extension direction show initial oblique-slip on traverse faults before orthogonal sets of dip-slip normal faults activate and accommodate extension during later rift stages (Corti, 2008; Agostini et al., 2009; Brune, 2014), although some earlier formed transverse faults may also be characterized by dip-slip motions (Corti et al., 2013; Philippon et al., 2015). However, the orientations of some joint sets measured by Atmaoui and Hollnack (2003) deviated significantly from fractures measured across the rest of the basin (Fig. 2). Specifically, a dominant NNW-trending (transverse) joint set was recorded in the vicinity of the transverse Kordjya fault. This is counter-intuitive given that joints theoretically form normal to σ_3 (Anderson, 1951; Pollard and Aydin, 1988), which has been proposed to be oriented WNW-ESE across the basin (Ibs-von Seht et al., 2001; Saria et al., 2014). The Magadi basin is also in a transitional phase in its development in that the locus of strain (i.e., magmatism and faulting) has recently begun migrating from the rift borders to the rift center (Muirhead et al., 2016; Weinstein et al., 2017), raising the question of whether the Kordjya fault formed in response to this recent change in rift system dynamics. These considerations regarding the timing and kinematics of the Kordjya fault contrast with past interpretations (e.g., Smith and Mosley, 1993; Atmaoui and Hollnack, 2003) and motivate a revision of the mechanics of transverse faulting in the Magadi basin of the Kenya Rift. Specifically, this study focuses on the timing of the Kordjya fault with respect to the dominant rift-parallel fault fabric. We provide a revised kinematic model for this transverse fault by considering the roles of inherited basement weaknesses, magmatism, magmatic volatile release, and the effects of evolving rift basin architecture on the activation of transverse faulting in the Magadi basin.

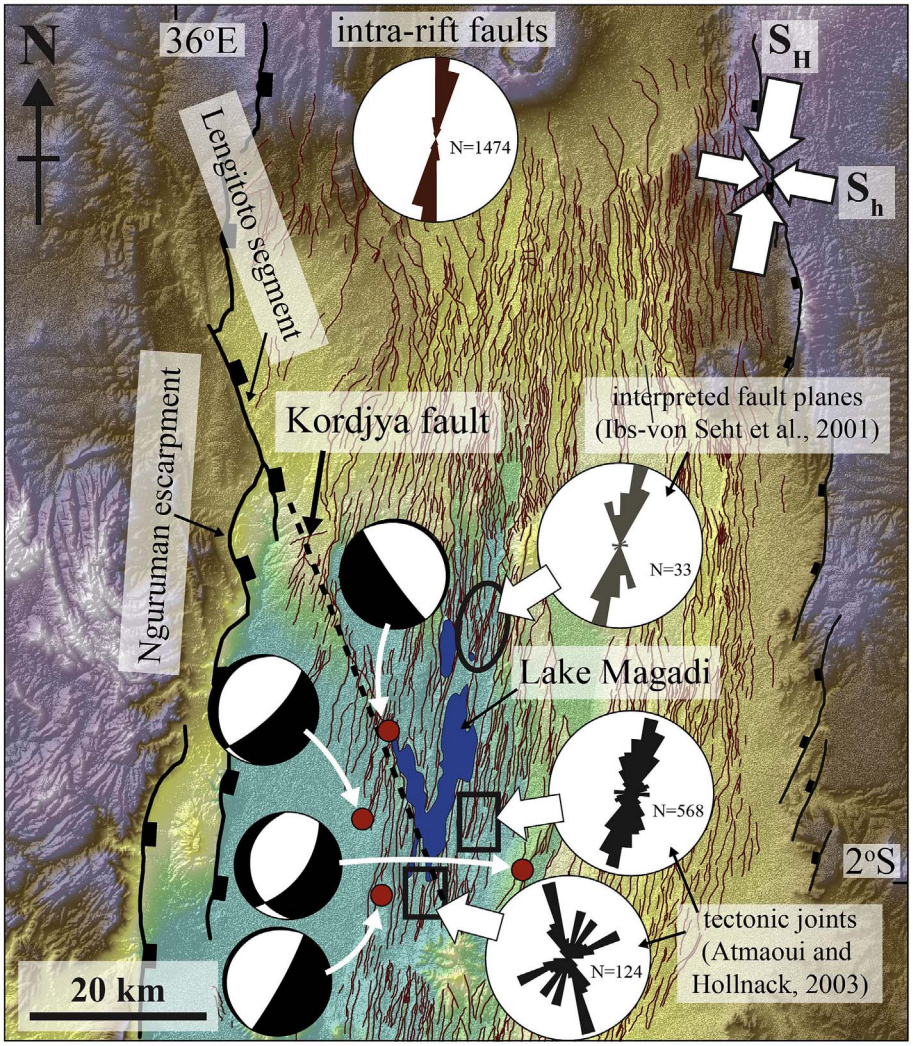

Fig. 2. Structural data from the Magadi Basin of the Kenya Rift (for the location, refer to Fig. 1B). Fault traces were mapped by Muirhead et al. (2016) using 0.5 m resolution aerial photography. Thick black lines represent the western border fault (Nguruman Escarpment), whereas thin black lines show the eastern boundary fault (Ngong-Turoka fault; Baker and Mitchell, 1976). Red lines represent intra-rift fault traces, and the strikes of these faults are presented in the rose diagram with red petals. Strikes of fault planes (primarily dip-slip normal faults) from Ibs-von Seht et al. (2001), presented in the rose diagram with grey petals, were interpreted from 33 focal mechanisms acquired from the 1998 seismic swarm in the center of the Magadi Basin. Focal mechanism for earthquakes within 10 km of the Kordjya fault from Weinstein et al. (2017) are also include, with locations indicated by red dots. The strikes of tectonic joints measured by Atmaoui and Hollnack (2003) in two sites in the Magadi basin are presented in the rose diagrams with black petals. The orientations of the greatest (S_H) and least (S_h) horizontal compressive stress, based on data from Ibs-von Seht et al. (2001) and Atmaoui and Hollnack (2003), are illustrated with white arrows. The trace of the Kordjya fault (dashed black line) is from Atmaoui and Hollnack (2003). This fault trace lines up with the Lengitoto border fault segment and forms part of the Engorika-Magadi-Lembolos structural lineament (Fig. 1B). Areas of highest elevation are colored white, whereas lowest elevation areas are colored green (see also 1C for elevations in the basin). (For interpretation of the references to colour in this figure legend, the reader is referred to the web version of this article.)

3. Field observations and remote-sensing analysis of the Kordjya fault system

3.1. Methods

Fault segment traces and throws were measured along the Kordjya fault (Fig. 3A) from high-resolution aerial photography (0.5 m/pixel) and Shuttle Radar Topography Mission (SRTM) data (30 m horizontal resolution, 7.6 m vertical precision; Rodríguez et al., 2005). The methods for measuring fault throw in the region, and associated uncertainties, are discussed in detail in Muirhead et al. (2016). In the current study, throw values represent the height of visible, surficial fault scarps measured using the 30 m SRTM dataset. Consistent with the method of Atmaoui and Hollnack (2003), the strikes of joints (lengths > 5 m) were measured in the field in Late Pleistocene to Holocene sediments and on faulted lavas within 50 m of fault scarps (Fig. 3A–C). To ensure we were not measuring joints formed from contraction related to cooling or desiccation (e,g., mud cracks), we measured only long joints (> 5 m) forming systematic sets with preferred orientations, and that also cut across polygonal cooling joints in lavas. Horizontal opening vectors were measured between matching piercing points (e.g., abrupt changes in strike) on opposing margins of dilational joints (Fig. 3D). Fault planes and rakes were also measured on (rare) striated fault-gouge sediments (Fig. 3E). Fault striations provided the sense of fault slip, assuming that all major faults in this extensional rift system exhibit a component of normal dip-slip (i.e., Ibs-von Seht et al., 2001; Weinstein et al., 2017, Fig. 2). Horizontal opening vectors along joints were used to infer the orientation of σ_3; however, where no opening vectors or other kinematic indicators (i.e., dilational jogs (Fig. 3F) or tail cracks) were present, the extension direction (i.e., σ_3) was inferred to be perpendicular to joint strike (Pollard and Aydin, 1988).

3.2. General structure

The ~60-km-long Kordjya fault has a maximum throw of 315.1 ± 10.7 m and displaces 0.95 to 1.37 Ma Magadi trachyte lavas (Muirhead et al., 2016). Assuming an optimal fault dip of 60°, these fault throw and age data correspond to a minimum time-averaged slip rate of 0.26–0.40 mm yr-1, consistent with slip rates (typically 0.1–4 mm yr-1) along major normal faults in extensional systems elsewhere. Examples include the Wasatch, Lake Tahoe, Campo Felice, Rangipo, and Paeroa faults of the Basin and Range (USA; Machette et al., 1991; Zhang et al., 1999; Hetzel and Hampel, 2005; Kent et al., 2005), Taupo Rift (New Zealand; Villamor and Berryman, 2001, 2006; Berryman et al., 2008; Downs et al., 2014), and Central Apennines (Italy; Galadini and Galli, 2000; Wilkinson et al., 2015). The throw-length ratio of the Kordjya fault system (0.0053) is consistent with ratios produced by normal faults dissecting rift lavas elsewhere (e.g., Iceland; Gudmundsson, 1992; Angelier et al., 1997), as well as regional data from the Natron and Magadi basins, which exhibit a mean throw-length ratio of 0.0059 for all measured faults (Muirhead et al., 2016).

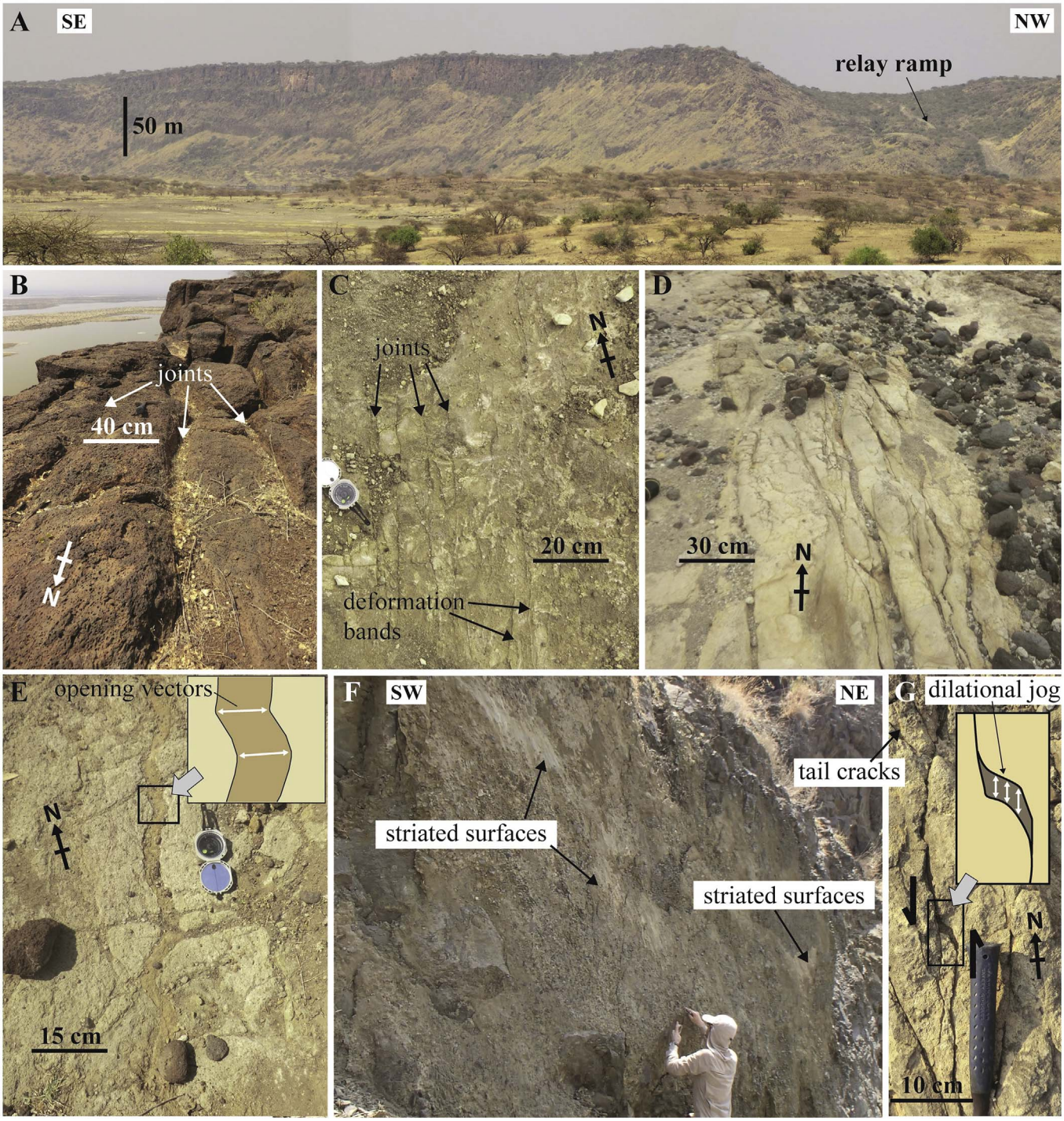

Fig. 3. Photos of structural features mapped in the field. A: View to the southwest of the northern end of a segment of the Kordjya fault (Segment 1 in Fig. 7) (photo location 1°49′38.51″S, 36°13′41.08″E). B: Tectonic joints near the footwall cutoff of the Kordjya fault in Magadi trachyte lavas (photo location: 1°51′40.01″S, 36°13′05.19″E). C: Rift-parallel joints and deformation bands in Late Pleistocene sediments (photo location: 2°01′05.60″S, 36°13′56.33″E). D: NNW-trending tectonic joints in the hanging wall of the Kordjya fault in Late Pleistocene sediments (photo location: 1°49′32.59″S, 36°12′10.94″E). E: Sediment-filled joint (photo location: 1°50′06.50″S, 36°12′06.12″E). Inset shows the dilation vector based on piercing points between matching fracture walls. F: Striated fault surface of a rift-parallel fault segment adjacent to the Kordjya fault, showing sinistral oblique-normal motion (rake = 70°N; photo location: 1°51′10.66″S, 36°12′59.57″E). G: Kinematic indicators (dilational jog and tailcracks) on NNE-trending joints (extensional-shear fractures) near the Kordjya fault, revealing a component of sinistral shear (photo location: 1°49′32.92″S, 36°12′11.25″E).

The Kordjya fault was previously mapped as a continuous NNW-trending fault (e.g., Atmaoui and Hollnack, 2003). However, our analysis indicates that the Kordjya fault consists of a complex system of predominantly NNE-striking, rift-parallel fault segments that collectively form a NNW-trending array of en echelon faults (Figs. 2 and 4). In all, the Kordjya fault is made up of 32 segments that form a roughly 60-km-long system. These segments merge into the main fault trace of the NNW-trending Kordjya fault (dashed line in Fig. 2A), hereafter termed the *main Kordjya fault*. Segments can be east- or west-facing (black and grey polygons, respectively, in Fig. 4A). Although fault segments are primarily rift-parallel, a few shorter (up to ~4 km-long) NNW-striking segments are present along the main Kordjya fault, suggesting the

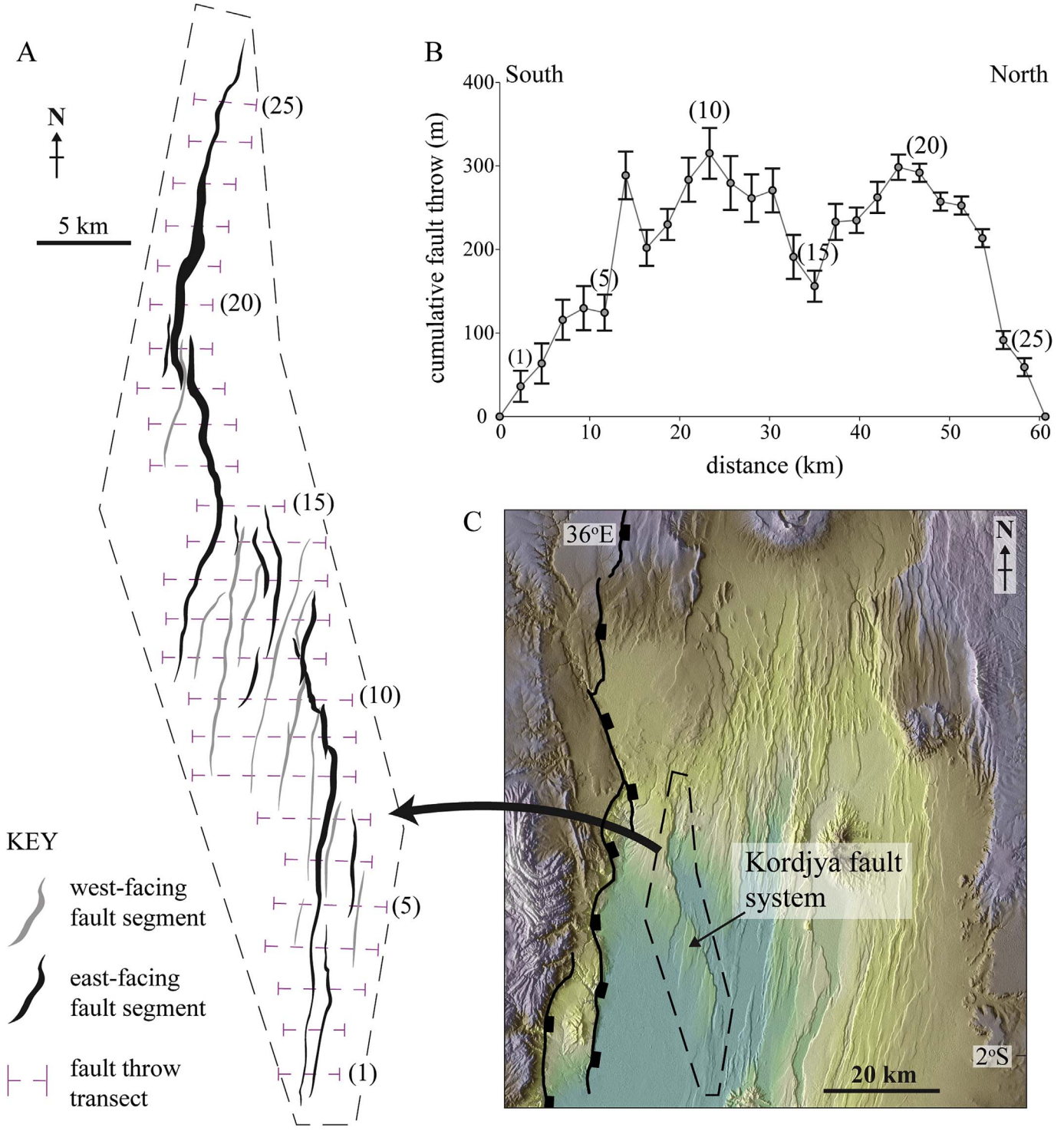

Fig. 4. A: Fault polygon map of the Kordjya fault system, comprising numerous rift-parallel fault segments aligned in a NNW-trending, en echelon pattern. East- and west-facing segments were mapped from an SRTM hillshade, and polygon thicknesses represent heave components of the fault scarps (i.e., a proxy for throw distribution, although also influenced by scarp degradation). Cumulative fault throws were measured along 25 ~E-W transects, shown as purple dashed lines. Only the major segments, with heaves visible in the 30 m SRTM, are included in this map. Dashed black polygon corresponds to the area demarcated in C. B: Fault throw distribution along the Kordjya fault, showing composite elliptical profiles consistent with a geometrically coherent system. Each throw value represents the cumulative throw measured along each transect in A. Numbers correspond to numbered transects in A. Error bars are to 95% confidence. C: Annotated SRTM map of the Magadi basin showing the location of the Kordjya fault system. The Nguruman border fault escarpment is annotated as a bold black line. (For interpretation of the references to colour in this figure legend, the reader is referred to the web version of this article.)

Kordjya fault may be starting to form a through-going structure that could potentially by-pass the original en echelon, rift-parallel segments, which it currently exploits.

To test whether these rift-parallel faults are kinematically coherent (Walsh and Watterson, 1988), the distribution of fault throw was analyzed from cumulative throw data collected along 25 E-W transects throughout the inferred system. The throws of faults were summed where they intersect each transect line (purple dashed lines in Fig. 4A). This approach reveals a throw profile comprising two adjacent elliptical segments. Together these segments form the larger Kordjya fault

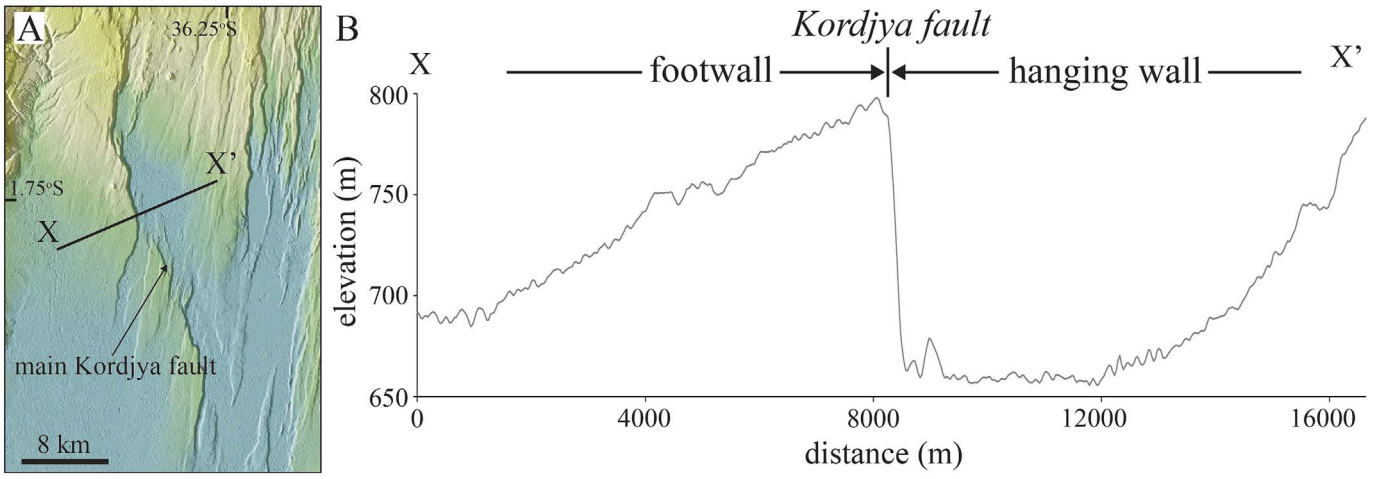

Fig. 5. A: Annotated SRTM map of the Magadi basin showing the location of the main Kordjya fault. The black line marked X-X′ refers to the location of the elevation profile in B. B: Elevation profile perpendicular to the main Kordjya fault (35 × vertical exaggeration). The elevation profile across the footwall, showing the topography gently dipping away from the fault, is consistent with the footwall profile of a normal fault. Similarly, the elevation profile across the hanging wall, where the topography gently dips towards the fault, is consistent with the hanging wall of normal a fault (e.g., Ebinger et al., 1991; Bott, 1996). The elevation increase on the right side of the profile marks a transition into the footwall uplift of an adjacent fault.

system, which is also defined by a broad elliptical throw profile. In all, these throw patterns suggest that the Kordjya fault is defined by two soft-linked, kinematically-coherent segments (Walsh and Watterson, 1988; Dawers et al., 1993; Cartwright et al., 1995; Nicol et al., 1996; Kattenhorn et al., 2016), that are themselves a composite of multiple NNE-SSW-striking normal fault segments (Fig. 4B). The two major soft-linked segments that define the Kordjya fault are also evident on fault segment and DEM maps presented in Fig. 4A and C.

Elevation profiles perpendicular to the strike of the Kordjya fault reveal a topographic profile consistent with the footwalls and hanging walls of normal faults observed from field and numerical modeling studies (Ebinger et al., 1991; Bott, 1996; Grant and Kattenhorn, 2004). For example, the ground surface gently dips away from the Kordjya fault scarp on the footwall side (Fig. 5), whereas on the hanging wall side, the ground surface gently dips toward the fault scarp. At the southeastern end of the main Kordjya fault, sets of fault-parallel springs emanate from the base of the fault scarp, providing the primary source of water into perennial Lake Magadi on the hanging wall side of the fault (Fig. 6; Lee et al., 2016; Muirhead et al., 2016).

Throw profiles were analyzed along all individual rift-parallel fault segments comprising the Kordjya fault that have maximum throws exceeding 25 m (n = 10) (Fig. 7). Although the entire Kordjya fault system collectively exhibits a composite of two merged elliptical throw profiles (merging at transect 15 in Fig. 4B), throw profiles along the individual rift-parallel fault segments that comprise the Kordjya fault are asymmetric (Fig. 7B). Maximum fault throws occur near the intersection of these segments with the main Kordjya fault (yellow stars in Fig. 7A). Here, the rift-parallel fault segments have begun to interact and link with one another, and exhibit both hard- and soft-linked relay zones (Gibbs, 1984; Childs et al., 1996). Soft-linked segments show no physical linkages between one another, yet are kinematically coherent (Walsh and Watterson, 1991) (Fig. 4). They exhibit relatively high throw gradients upon intersecting the main Kordjya fault, with throw quickly decreasing from the maximum value to zero at fault tips (e.g., the northern ends of Segments 2 and 8 in Fig. 7). Fault throws for hard-linked segments, however, do not reduce to zero, as they exhibit identifiable connections with adjacent segments across the main Kordjya fault (e.g., northern end of Segment 1 in Fig. 7). Some rift-parallel segments also interact with shorter NNW-trending segments that have begun to develop a through-going, transverse fault trace. At rare localities, segments do not appear to interact directly with neighboring segments as they cross the main Kordjya fault. For example, segment 10 of Fig. 7 can be traced across the main Kordjya fault into the hanging wall side. However, its maximum throw still occurs at its intersection with the main Kordjya fault, as occurs in all other rift-parallel segments forming the Kordjya fault system.

Many rift-parallel fault segments terminating near the main Kordjya fault exhibit curved ends (in a counter-clockwise sense) reminiscent of tailcracks (Cruikshank et al., 1991; Willemse et al., 1997; Marshall and Kattenhorn, 2005; Watkinson and Ward, 2006) (Fig. 8). Curved ends are not present at distal fault tips occurring away from the main Kordjya fault (e.g., southern end of Segment 1, Fig. 7). Field and modeling studies show that fault tip geometries can be used as kinematic indicators of the sense of slip, specifically to determine if fault motion is characterized by a component of sinistral or dextral shear (Pollard and Aydin, 1988; Cruikshank et al., 1991; Kattenhorn, 2004). Left-curving (counter-clockwise rotation) and right-curving (clockwise rotation) tailcracks indicate a component sinistral shear and dextral shear, respectively. The ends of many rift-parallel faults intersecting the main Kordjya fault exhibit left-curving geometries, which suggest a component of sinistral shear in addition to the predominantly dip-slip motions expected along these oblique-normal faults (Fig. 8).

3.3. Fault kinematic indicators from field observations

Systematic joint sets and rare deformation bands (~1 mm-wide) were analyzed along and around the Kordjya fault system (Figs. 3 and 9). Occasionally, tectonic joints (< 4-cm-wide) are filled with very fine-grained sediment (Fig. 3D). Consistent with previous studies on tectonic joints in the region (Atmaoui and Hollnack, 2003), two dominant joint sets and two sets of horizontal opening vectors are observed (Fig. 9D). NNE-trending joints (locations v-vii in Fig. 9A) are observed away from the main Kordjya fault (pink rectangle in Fig. 7), and are consistently present throughout the Magadi basin (Atmaoui and Hollnack, 2003). These tectonic joints trend parallel to rift-parallel faults throughout the Magadi basin (intra-rift faults in Fig. 2A) and exhibit a mean opening vector of 115°, which is consistent with previous estimates of the regional extensional direction (105–115°) from investigations of joints and focal plane mechanism (Ibs-von Seht et al., 2001; Atmaoui and Hollnack, 2003; Weinstein et al., 2017) (Fig. 2). However, in the vicinity of the main Kordjya fault, a second, NNW-trending joint set is present (locations i, iii, and iv in Fig. 9A). Rare N- to NNE-trending joints observed here exhibit dilational jogs and left-curving tailcracks, consistent with a component of left-lateral shear (Fig. 3F). Opening

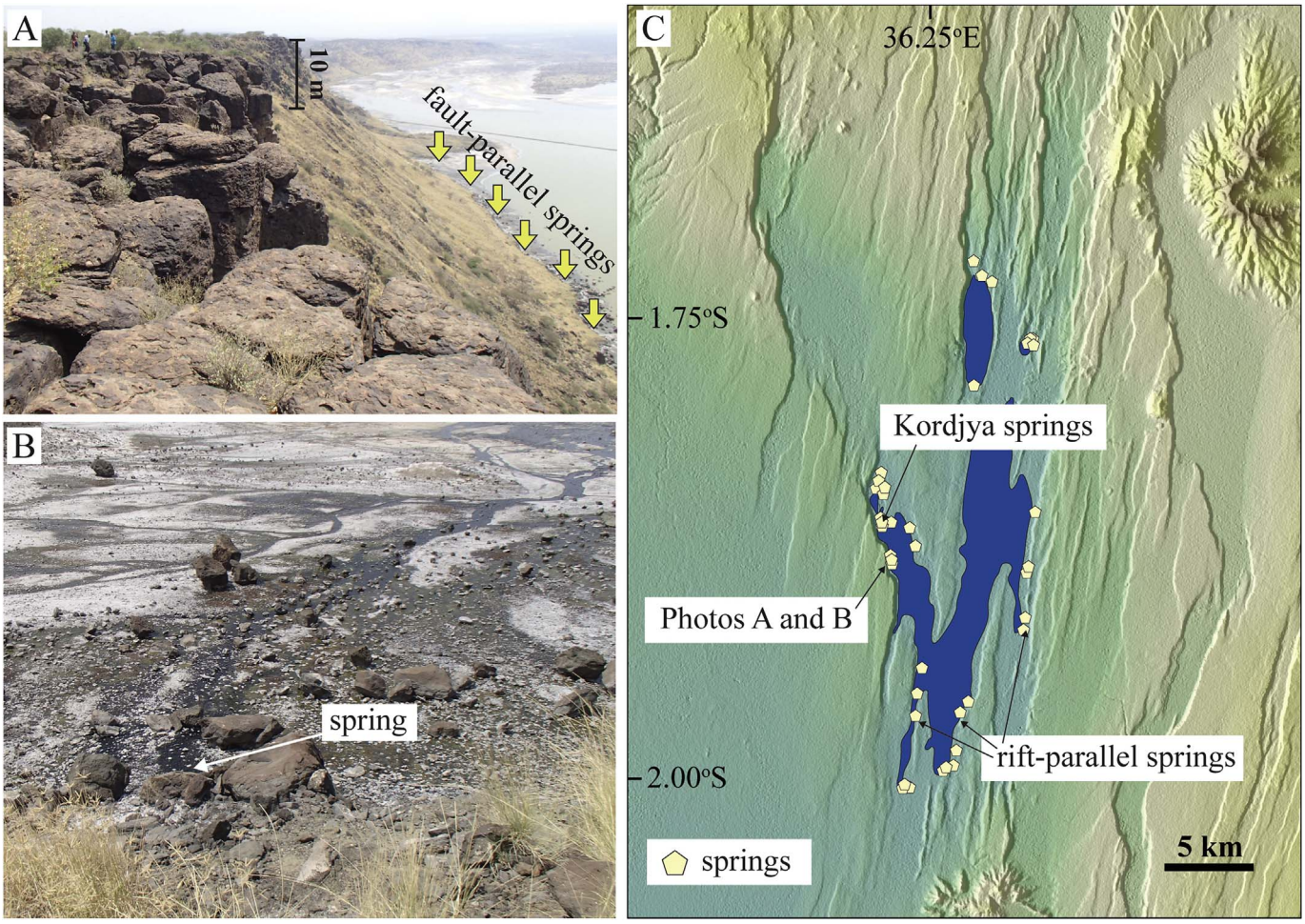

Fig. 6. Distribution of springs along the Kordjya fault and Lake Magadi. Spring locations are based on observations from this study and data from Baker (1963). A: Photo to the NNW of the Kordjya fault (location annotated in C). The height of the fault scarp here is ~154 m. B: Photo to NE of a spring at the base of the Kordjya fault. Springs here flow ENE into Lake Magadi. C: Annotated SRTM image of the center of the Magadi basin showing the distribution of springs (from Muirhead et al. (2016)) and lake waters (dark blue polygon). Most springs occur along rift-parallel faults in the axial depression of the Magadi basin; however, over a third of the springs emanate from the transverse Kordja fault. (For interpretation of the references to colour in this figure legend, the reader is referred to the web version of this article.)

vectors measured on NNW-trending joints exhibit a mean opening direction of 079° (refer to location iii in Fig. 9A), which is normal to the mean joint orientation and the main Kordjya fault trace, but oblique to the regional extension direction. Measured fault surfaces on rift-parallel faults intersecting the main Kordjya fault exhibit strikes and dips ranging 015–025° and 78–87°, respectively (location ii in Fig. 9A). Striations on these surfaces exhibit rakes of 70°N, consistent with a sinistral component of shear along NNE-trending rift-parallel faults in the vicinity of the Kordjya fault. Overall, joint and fault kinematic data (locations i-iv in Fig. 9) support ENE-WSW extension in the vicinity of the main Kordjya fault, which would likely produce dip-slip motion on a NNW-trending fault structure such as the Kordjya fault, consistent with its throw characteristics (Fig. 5), and focal mechanisms from earthquake events tracing along the main Kordjya fault (Weinstein et al., 2017) (Fig. 2).

4. Discussion

4.1. Kinematics and timing of faulting in the Kordjya system

To create a conceptual kinematic model for the Kordjya fault system, it is important to consider the mechanics of the rift-parallel fault segments (Fig. 10) and their role in facilitating the evolution of the main Kordjya fault. Our analysis of rift-parallel faults and joints alongside the main Kordjya fault reveals a complex kinematic model for some rift-parallel faults in the Magadi basin (Fig. 9). Fault tip zone geometries, slip vectors, and dilational jogs observed on (rare) NNE-striking joints (Figs. 3, 8 and 9) are consistent with a component of left-lateral shear along NNE-striking extensional structures near the main Kordjya fault. Joint sets here dominantly trend NNW, rather than the NNE, and exhibit ENE-trending dilation vectors, which suggests ENE-WSW extension in the vicinity of the main Kordjya fault. This extension direction is consistent with the kinematic indicators of left-lateral shear observed along the NNE-striking rift-parallel fault segments (Fig. 10). Moreover, fault tip zone geometries, slip vectors, and dilational jogs observed on rare NNE-striking joints within the fault zone of the main Kordjya fault (Figs. 3, 8 and 9) are consistent with a component of left-lateral shear.

A change in the kinematic behavior of rift-parallel faults in the vicinity of the main Kordjya fault is further supported by the asymmetric nature of analyzed fault throw profiles (Figs. 7 and 10). Specifically, the maximum fault throws along these rift-parallel faults all correspond to where they intersect the main Kordjya fault (pink polygon in Fig. 7), suggesting that activity along the Kordjya fault system locally reactivated these rift-parallel structures with focused sinistral-oblique-normal slip activity where these faults intersect the main Kordjya fault trace (Figs. 7 and 10). The implication is that these rift-parallel faults formed prior to the development of the Kordjya fault, in response to the regional ESE-WNW extension (Fig. 11). This interpretation is further supported by the overall nature of segmentation in the Kordjya fault

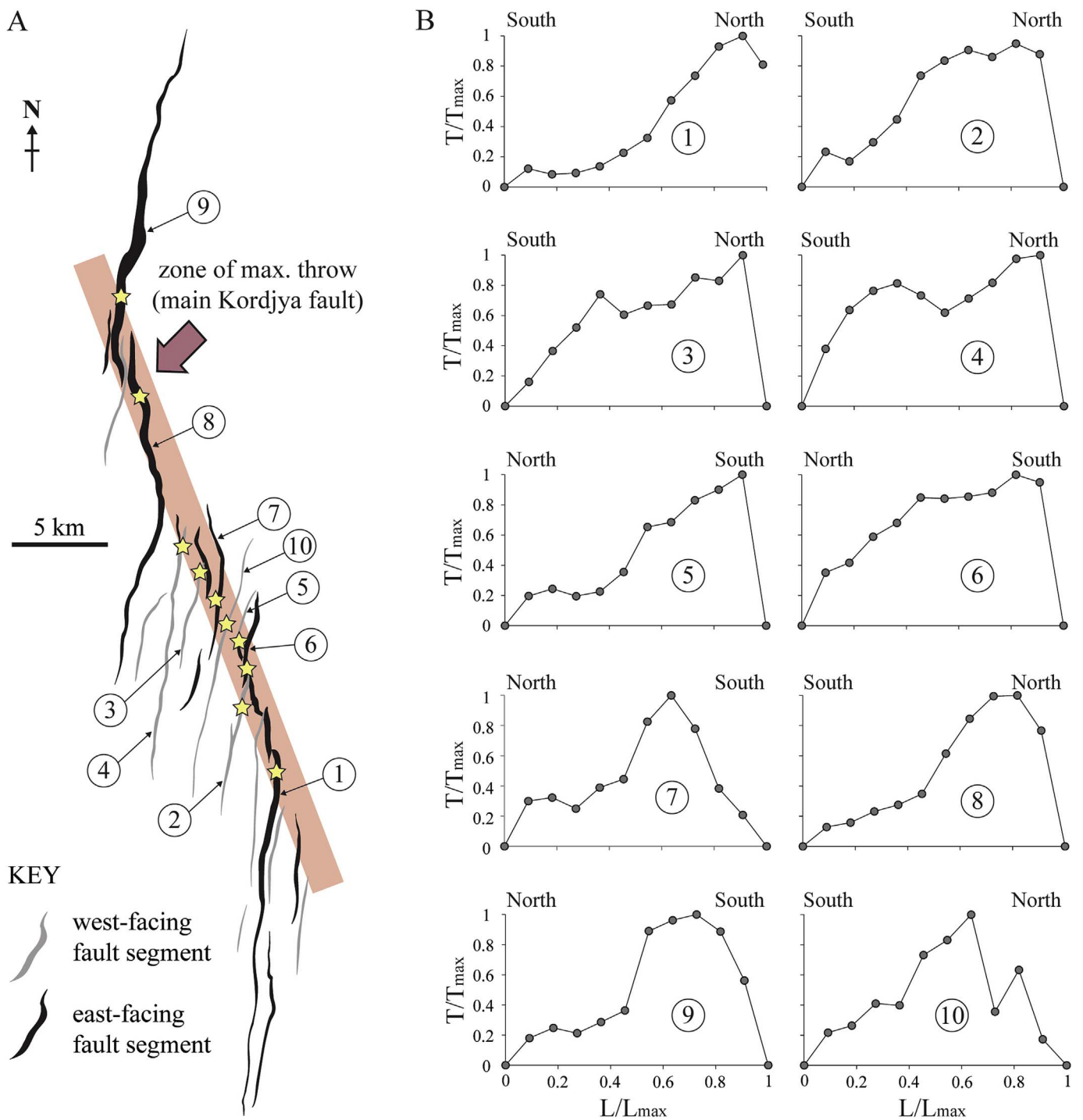

Fig. 7. Distribution of fault throw along rift-parallel segments that comprise the NNW-trending Kordjya fault system. A: Map view of rift-parallel fault segments (see Fig. 4C for location). East- and west-dipping segments were mapped from an SRTM hillshade, and line thickness corresponds to the fault scarp width (i.e., fault heave). Numbers correspond to fault throw profiles shown in B. The location of maximum fault throw for each analyzed segment is shown as a yellow-filled star, and defines a NNW-trending zone (pink rectangle) that follows the trace of the main Kordjya fault (see Fig. 2A). B: Fault throw data collected along rift-parallel fault segments. Numbers correspond to faults annotated in A. Throw (T) and length (L) data in each plot are normalized by the maximum throw (T_{max}) and length (L_{max}) values, respectively, along each fault. Faults exhibit asymmetric throw profiles with maximum throw values occurring along the trace of the main Kordjya fault. Hard-linked faults exhibit non-zero throw values at fault tips. (For interpretation of the references to colour in this figure legend, the reader is referred to the web version of this article.)

system. If the NNW-trending Kordjya fault predated the rift-parallel fault system, we would expect it to form a through-going structure optimally oriented normal to the local, WSW-ENE extension direction. Under this scenario, slip along the Kordjya fault wouldn't require re-activation of the NNE-SSW-striking, rift-parallel faults. As displacements along the Kordjya fault require reactivation of non-optimally oriented, yet kinematically-coherent, rift-parallel faults, it is therefore more likely that this fault post-dates the rift-parallel fabric.

Once the rift-parallel fault fabric was established in 0.95–1.37 Ma Magadi trachyte lavas (Muirhead et al., 2016), the Kordjya fault system was initiated, possibly from the reactivation of the NNW-trending Aswa basement shear zone (Smith and Mosley, 1993; Smith, 1994; Le Turdu et al., 1999) (Fig. 11D and E). The reactivation of this basement fabric probably occurred in response to a localized shift in the orientation of

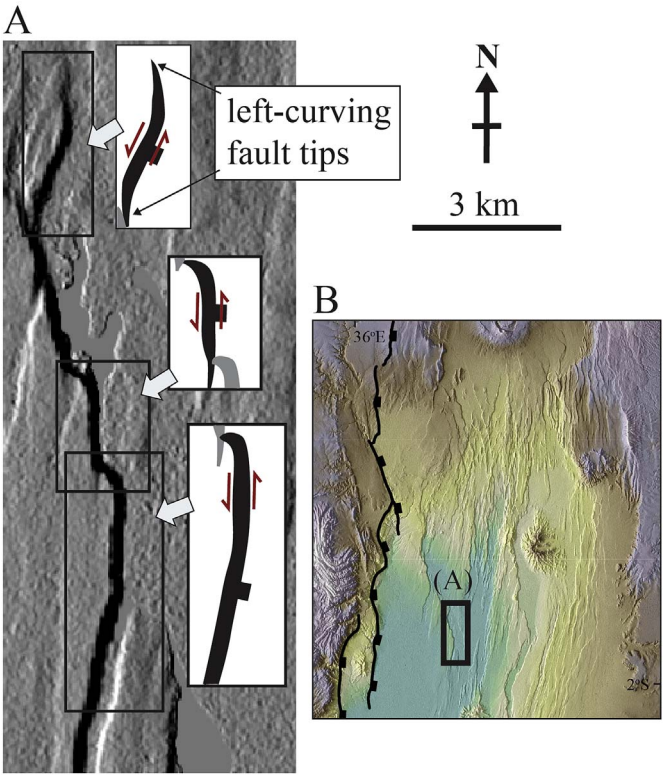

Fig. 8. A: Annotated SRTM hillshade (lighting from the W) showing east-dipping rift-parallel faults terminating at the main Kordjya fault (scale bar in the top right). N- to NNE-trending fault segments exhibit left-curving tip zones indicative of a component of sinistral shear (red arrows). B: Location of A in the Magadi basin. (For interpretation of the references to colour in this figure legend, the reader is referred to the web version of this article.)

σ_3 from ESE-WNW to ENE-WSW, which optimally oriented NNW-trending basement fabrics with respect to this (local) stress field. The WSW-ENE extension inferred from field data is expected to translate to dip-slip motion along a NNW-trending structure at basement depths (Fig. 11E). The earlier formed rift-parallel structures in the vicinity of the Kordjya fault were thus reactivated as oblique-normal faults with a component of left-lateral shear in order to accommodate dip-slip motion along this NNW-trending fault (Fig. 12), resulting in polyphase fault activity along an inherited structural fabric (e.g., Kattenhorn et al., 2016).

We reject the possibility that the sinistral-oblique motions inferred for the en echelon, rift-parallel faults resulted from bookshelf style faulting (e.g., Sigmundsson et al., 1995) that could theoretically accommodate dextral shear along the transverse Kordjya fault within the crystalline basement. Dextral shear along the NNW-trending transverse structure would result from E-W to ESE-WNW extension in the vicinity of the Kordjya fault; however, this extension direction is not consistent with kinematic data presented in this study (Fig. 9), nor in previous work (Atmaoui and Hollnack, 2003, Fig. 2). Instead, the local orientation of σ_3 (WSW-ENE) and topographic profiles across the footwall and hanging wall of the NNW-trending main Kordjya fault are consistent with normal faulting (Figs. 5 and 9). Therefore, we maintain that the most consistent model is that of dip-slip faulting at basement depths resulting from a counterclockwise rotation of σ_3 in the vicinity of the main Kordjya fault (Fig. 11E).

4.2. An alternative model for transverse faulting in the Magadi basin

The revised kinematic model for the Kordjya fault system presented here (Figs. 11 and 12) contrasts with previous assertions of the timing and kinematics of transverse faulting in the Kenya Rift. Previous studies in the Magadi area have suggested that NNE-striking, rift-parallel faults across the Magadi basin exhibit dip-slip kinematics, whereas NNW-trending transverse structures act as oblique-normal faults with a component of dextral shear (Smith and Mosley, 1993; Le Turdu et al., 1999; Atmaoui and Hollnack, 2003). Many studies also favor the reactivation of preexisting weaknesses during the initiation of rifting (Versfelt and Rosendahl, 1989; Chorowicz, 1992; Chorowicz and Sorlien, 1992; Modisi et al., 2000; Agostini et al., 2009). In the Kenya Rift specifically, transverse faults are thought to reactivate NNW-trending basement weaknesses (Mosley, 1993), and fail with a component of dextral shear in order to accommodate regional ESE-WNW extension (Smith and Mosley, 1993; Le Turdu et al., 1999; Atmaoui and Hollnack, 2003). Over the course of rift evolution, transverse faults in the EARS should theoretically be abandoned as more favorably oriented rift-parallel faults develop and the lithosphere weakens via heating and stretching (Chorowicz and Sorlien, 1992; Ebinger, 2005; Corti, 2008; Agostini et al., 2009; Brune, 2014).

In contrast, the reactivation of NNE-trending structures by the Kordjya fault system suggests that these rift-parallel faults, which formed in response to regional ESE-WNW extension, actually developed prior to the activation of the present day NNW-trending transverse fault (Fig. 11C). These earlier formed rift-parallel faults created an inherited structural fabric that was subsequently cannibalized by the developing transverse Kordjya fault. Field kinematic data favor dip-slip fault kinematics on the transverse Kordjya fault, whereas rift-parallel faults ultimately developed sinistral-oblique-normal slip kinematics in order to accommodate localized ENE-WSW extension (Fig. 12).

The revised kinematic model supports the assertions of recent studies that many apparently transverse faults across the EARS exhibit dip-slip kinematics (e.g., Modisi et al., 2000; Delvaux and Barth, 2010; Morley, 2010; Delvaux et al., 2012; Corti et al., 2013). These studies inferred fault kinematics from focal plane mechanism, field kinematic indicators, and aeromagnetic data of displaced subsurface features (dikes), revealing dip-slip normal fault motions along major transverse structures. The reactivation of preexisting structures under these models is inferred to result from spatial and temporal variations in the direction of the regional σ_3 over the lifetime of the rift (Morley, 2010; Delvaux et al., 2012).

4.3. Reactivation of pre-existing weaknesses during rift evolution in the Magadi basin

Given the abundance of rift-parallel faults in the Magadi basin that prevailed during early rift evolution (i.e., since ~7 Ma) the recent tendency for dip-slip activity along transverse features like the Kordjya fault suggests a change in rift driving forces. Below we discuss how the development of the Kordjya fault possibly relates to evolving magma systems and rift basin tectonic architecture, including the interaction between first-order rift basin segments and inherited crustal weaknesses, as well as the temporally changing partitioning of fault strain within the rift basin.

The tectonic-magmatic development of the Magadi basin over the last 7 million years is comparable to existing conceptual models for basin evolution in the Eastern rift branch (see Muirhead et al., 2016, and references therein). These studies suggest that strain is initially accommodated along rift border faults before migrating toward the rift center, where regional extension is accommodated by magmatism and intra-rift faulting. Similarly, the initial stages of rifting in Magadi (~7-5 Ma) were characterized by faulting and volcanism along the rift borders (Fig. 13A). Faulting initiated on the Nguruman border fault escarpment at ~7 Ma, ultimately developing into a 1.6 km high escarpment (with ~5 km of total throw; Muirhead et al., 2016) and creating an asymmetric basin with a westward-dipping flexure. Border fault development was accompanied by the eruption of Lengitoto trachyte lavas (6.9–5.0 Ma) along the western rift edge (Crossley, 1979). Rift volcanism initiated on the eastern border of Magadi at ~6.7 Ma (Fig. 13A)

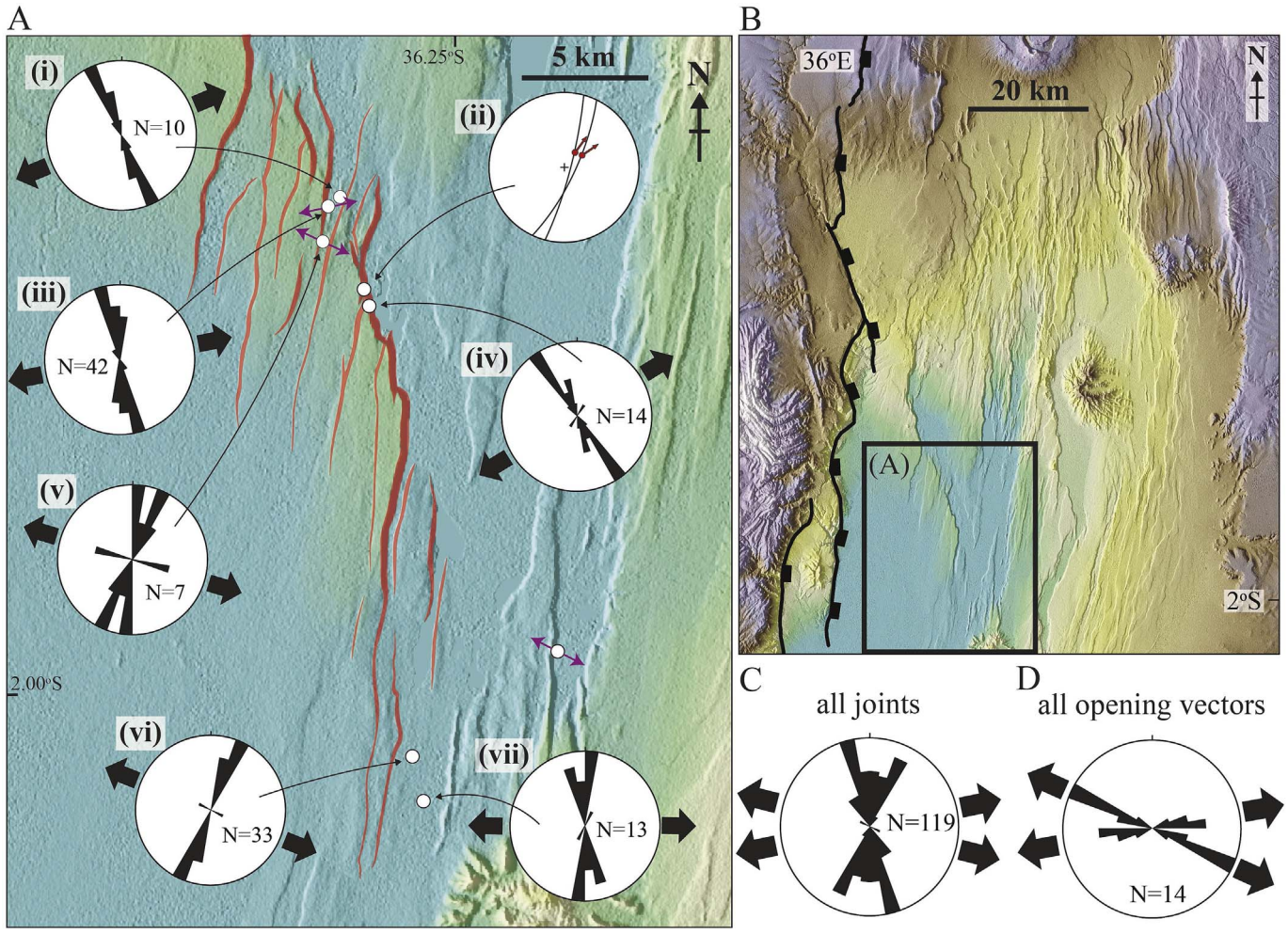

Fig. 9. A: Tectonic joint measurements around the Kordjya fault system. Sample locations (white circles) are annotated on an SRTM map of the Kordjya fault. Red polygons represent scarps of the Kordjya fault segments shown in Figs. 4 and 7. Rose plots show joint strikes at the six locations. Bold black arrows represent the inferred extension directions during original joint development, assumed to be normal to the mean trend of the tectonic joint set. Purple arrows represent the mean dilation vectors at selected locations. Also shown is a lower hemisphere stereonet plot of fault plane orientations (great circles) and slip vectors (red arrows) along the main Kordjya fault trace (location ii). Note the change in extension directions from ENE-WSW and NE-SW near the main Kordjya fault, to ESE-WNW and E-W south and east of the fault. B: Annotated SRTM map of the Magadi basin showing the location of the map in A. Nguruman border fault escarpment annotated as a bold black line. C: Rose plot of the strikes of all measured tectonic joints. Bold black arrows represent the inferred, disparate extension directions, assumed to be normal to the dominant NNW-trending and NNE-trending joint sets. D: Rose plot of all measured dilation vectors observed across joints. Bold black arrows represent the inferred, disparate extension directions. (For interpretation of the references to colour in this figure legend, the reader is referred to the web version of this article.)

with the eruption of Ol Eyaseti volcanics (Baker et al., 1971; Baker and Mitchell, 1976).

From 5 Ma onwards, volcanic activity was distributed across both the rift borders and the central rift axis (Fig. 13B), including the Ngong (2.5–2.6 Ma) composite volcano and related volcanics (Baker and Mitchell, 1976; Saggerson, 1991), as well as widespread lava eruptions of the Kirikiti and Limiru trachytes (5.1–2.5 and 2.05 Ma, respectively) (Baker et al., 1971; Crossley, 1979; Muirhead et al., 2016). The Ngong-Turoka fault escarpment, which bounds the eastern side of the basin, also developed during this period (2.3–3.3 Ma) (Baker and Mitchell, 1976).

Since ~2 Ma, however, volcanism and faulting in the Magadi basin became increasingly focused into the rift center (Fig. 13C). This transition was accompanied by emplacement of magmas below the central rift axis (inferred from gravity and seismic tomography data; Baker and Wohlenberg, 1971; Birt et al., 1997; Ibs-von Seht et al., 2001; Roecker et al., 2017; Weinstein et al., 2017), eruption of voluminous rift lavas (e.g., 295 km3 Magadi trachyte lavas; Guth, 2015), and release of magmatic volatiles along fault systems in the rift center (e.g., > 1 Mt yr-1 of magmatic CO_2; Lee et al., 2016, 2017). Together, these observations support a magmatic- and fluid-driven model of strain localization into the center of the rift (i.e., Ebinger and Casey, 2001; Keir et al., 2006; Beutel et al., 2010; Roecker et al., 2017), with some intra-rift faulting also resulting from extensional stresses in a flexing border fault hanging wall (Muirhead et al., 2016). The focusing of strain into the intra-rift fault system has resulted in basin subsidence along the central axis of the valley floor, creating the topographically lowest point within the rift valley (Fig. 13C), and forming a catchment basin for axial Lake Magadi since the Late Pleistocene (Behr and Rohricht, 2000; Muirhead et al., 2016).

The migration of strain toward the rift center in the Magadi basin represents a fundamental change in along-axis segmentation within this section of the rift (Weinstein et al., 2017). Developing rift segments in East Africa typically grow and link through along-axis propagation and subsequent interaction of fault and magmatic systems (e.g., Ebinger, 1989; San'kov et al., 2000, 2009; Densmore et al., 2007; Beutel et al., 2010; Allken et al., 2011; Muirhead et al., 2015; Wauthier et al., 2015). Emplacement of high-density, axial magmatic segments in evolving rifts drives downward crustal flexure (Corti et al., 2015), which can theoretically reorient local stress fields (e.g., Cailleau et al., 2003), and stresses may also reorient in the interaction zone between developing rift segments (Pollard and Aydin, 1984; Muirhead et al., 2015).

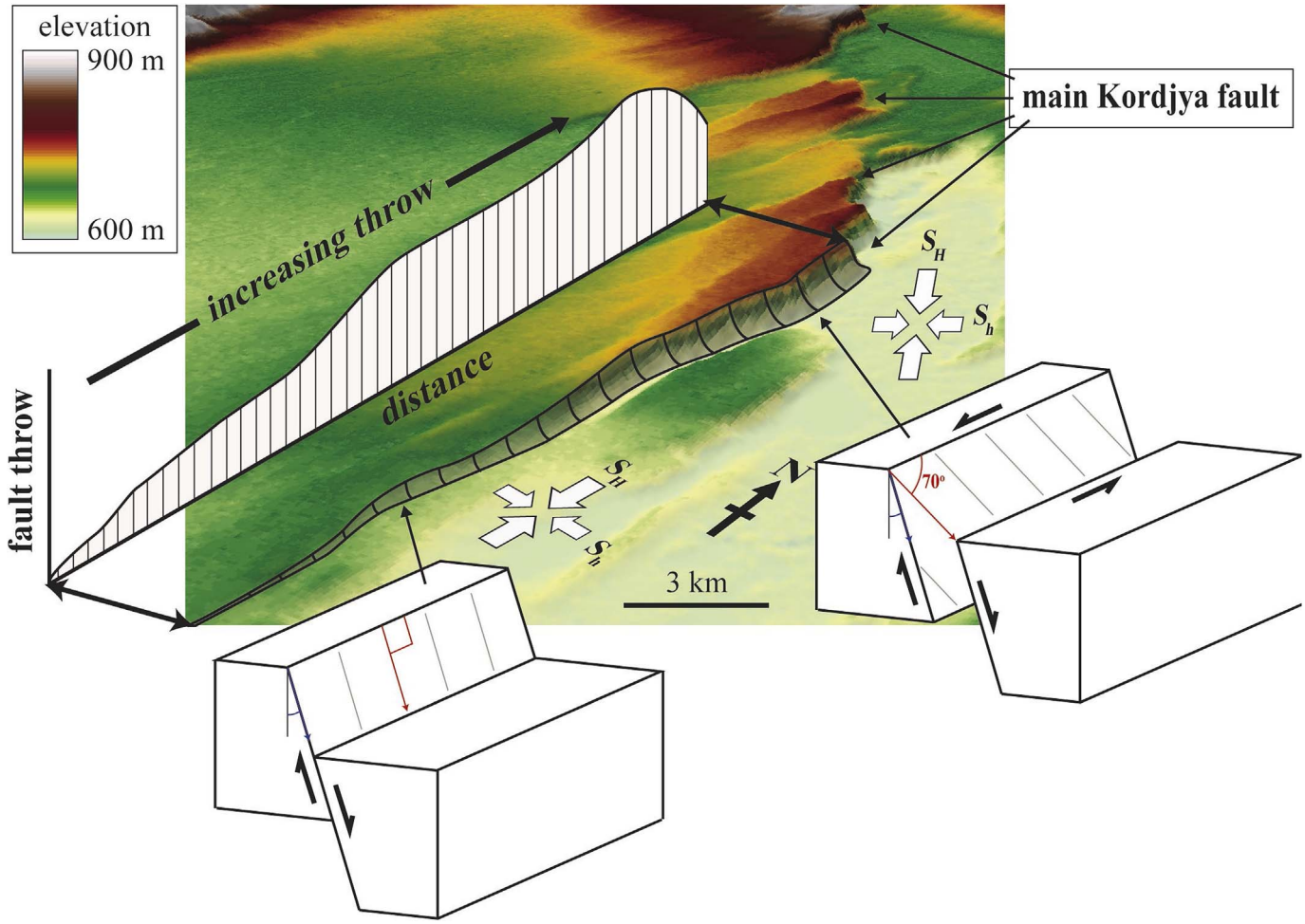

Fig. 10. Conceptual illustration of the kinematics of rift-parallel faults in the Kordjya fault system, annotated on a SRTM map (oblique-aerial view). The superposed idealized fault throw profile (see Fig. 7) shows the maximum fault throw where the rift-parallel fault approaches the main Kordjya fault. The corresponding fault scarp is shaded grey and outlined in black on the SRTM map. The orientations of the greatest (S_H) and least (S_h) horizontal compressive stress are based on joint and fault-slip data in Fig. 9. South of the main Kordjya fault, the least compressive stress is parallel to the ESE-WNW regional extension direction, but rotates in the vicinity of the main Kordjya fault, resulting in ENE-WSW extension. Conceptual block diagrams show along-strike changes in the sense of slip along rift-parallel faults based on inferred stress regimes and fault slip data collected in the field. South of the main Kordjya fault, NNE-trending rift-parallel faults exhibit pure dip-slip motions (slip vectors indicated by red arrows), whereas in the vicinity of the main Kordjya fault they exhibit oblique-slip with a component of sinistral shear. (For interpretation of the references to colour in this figure legend, the reader is referred to the web version of this article.)

Transverse fault zones that create physical and mechanical linkages between rift segments may subsequently develop, re-adjust, or become abandoned in response to rift propagation and evolution (e.g., Chorowicz, 1989; Ebinger, 1989; Morley et al., 1990; Modisi et al., 2000; Densmore et al., 2007; Koehn et al., 2010; Ebinger and Scholz, 2012). Consequently, new transverse faults can potentially reactivate preexisting fabrics during later stages of rifting as first-order rift segments develop and interact. Under this model, the reactivation of non-optimally-oriented, preexisting basement weaknesses may post-date the development of rift-parallel faults, with transverse structures forming at later stages of rift evolution (e.g., the transfer zones between intra-rift fault populations of Corti (2008) and Agostini et al. (2009)). Depending on how σ_3 reorients within interaction zones between newly developing rift segments (Pollard and Aydin, 1984; Muirhead et al., 2015), these transverse faults may also exhibit dip-slip kinematics (e.g., Koehn et al., 2010; Morley, 2010), rather than forming as the oblique-slip structures that are predicted during the reactivation of basement fabrics during rift initiation (e.g., Kilembe and Rosendahl, 1992; Ring et al., 1992; Smith and Mosley, 1993; Le Turdu et al., 1999).

Consistent with the studies described above, a number of lines of evidence suggest that the activation of the Kordjya fault occurred as a response to evolving rift segmentation in the Magadi basin (Fig. 13). First, the Kordjya fault system post-dates the formation of the rift-parallel faults in the rift center, which have accommodated a significant proportion of regional tectonic strain (67–80%) within the last ~1 million years (Muirhead et al., 2016). The Kordjya fault therefore initiated immediately after, or possibly with, the establishment of this new centralized region of magma- and fault-related strain accommodation at the center of the rift (Muirhead et al., 2016; Weinstein et al., 2017) (Fig. 13C). Second, the SE section of the main Kordjya fault merges into the axial depression (i.e., Lake Magadi) of the Magadi basin, into the northern portion of a developing magmatic segment interpreted by Weinstein et al. (2017). To the NW, the fault cuts across the dominant rift-parallel structural fabric, and can be traced into the Lengitoto segment of the border fault (Atmaoui and Hollnack, 2003, Fig. 2). This border fault segment shares the same orientation as the Kordjya fault and likely exploits the same NNW-striking basement weaknesses (Figs. 2A and 11E). The Kordjya fault is therefore inferred to connect the developing locus of strain in the rift center (i.e., developing magmatic segment of Weinstein et al. (2017)), with the previous locus of strain along the rift border. Third, the development of the Kordjya system is, in part, related to a counter-clockwise rotation of the local least compressive stress direction within the basin. The described counter-clockwise rotation of σ_3 is consistent with a mechanical interaction between offset, left-stepping rift basin segments; specifically, the developing magmatic segment below Lake Magadi (Weinstein et al.,

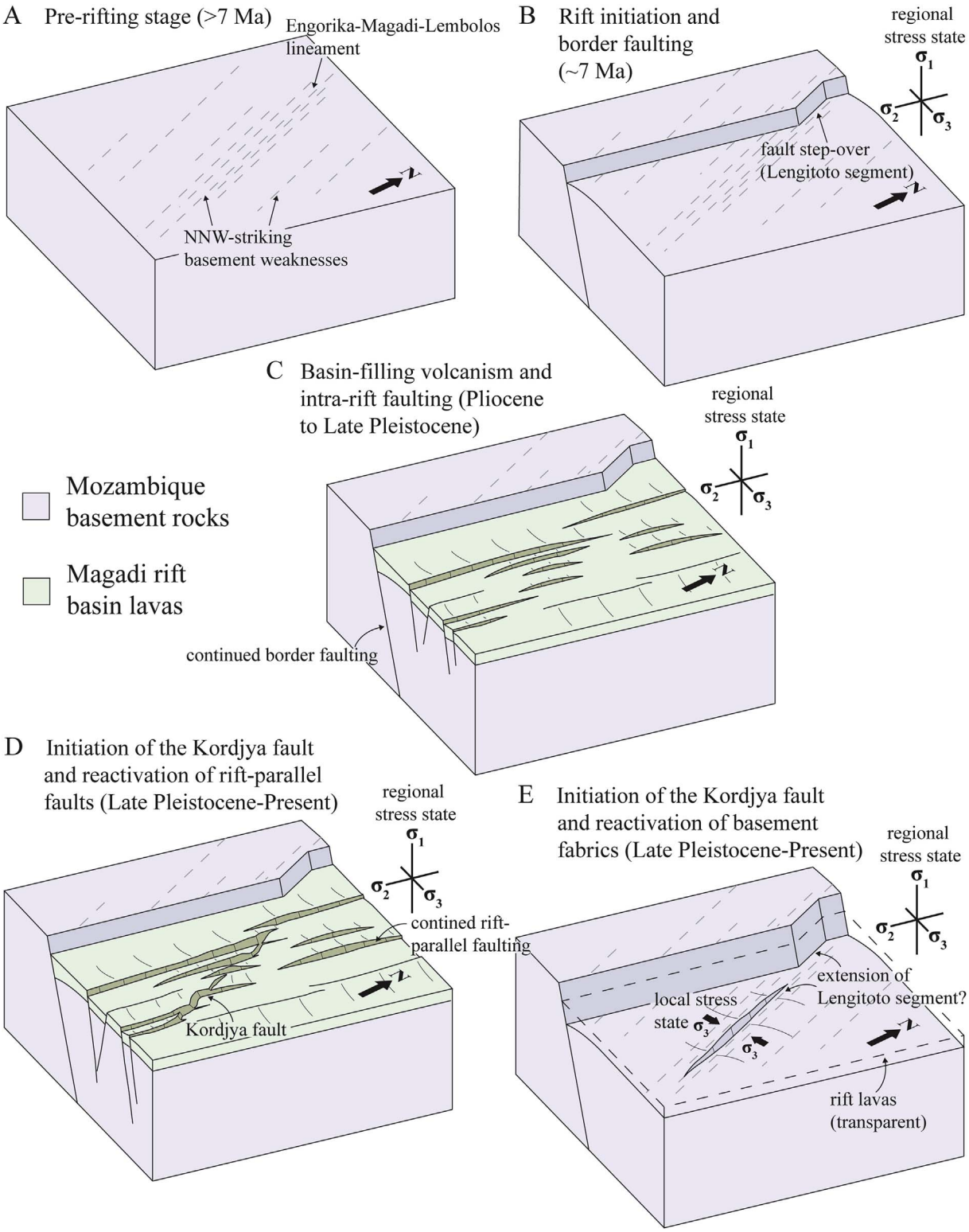

Fig. 11. Simplified model of the timing of border, rift-parallel, and transverse fault development in the Magadi basin. A: Prior to rifting, the area dominantly comprised Mozambique Belt basement rocks with NNW-striking shear fabrics of the Aswa shear zone (Smith and Mosley, 1993). B: Faulting along the Nguruman border fault initiated at ~7 Ma (Crossley, 1979). Segmentation along the border fault, and subsequent development of the Lengitoto segment, was controlled by NNW-striking, preexisting weaknesses in Mozambique Belt rocks. Specifically, the Lengitoto fault segment localized along the Engorika-Magadi-Lembolos structural lineament (shown in A). C: Following the development of the Nguruman border fault, the Magadi basin went through a phase of basin-filling volcanism and intra-rift faulting. The rift-parallel fault segments comprising the Kordjya fault today formed after the emplacement of Magadi trachyte lavas in the Mid-to Late Pleistocene. D: Initiation of the transverse Kordjya fault. A series of en echelon, rift-parallel faults were reactivated as sinistral-oblique-normal faults to produce a kinematically coherent, NNW-trending fault system. The Kordjya fault is aligned with both the nearby Lengitoto segment of the Nguruman border fault and the underlying Engorika-Magadi-Lembolos lineament, suggesting the Kordjya fault may be a response to reactivation of a long-lived, influential basement fabric. E: Inferred geometry of the Kordjya fault below syn-rift volcanics of the Magadi basin. The structure forms a through-going, NNW-trending, normal fault at depth, and effectively represents a SW extension of the Lengitoto border fault segment that effectively transfers extensional strain from the border fault into the center of the rift basin. The local orientation of σ_3 (bold black arrows) is inferred from field data in this study, and would result in dip-slip normal fault motion along a NNW-trending basement structure.

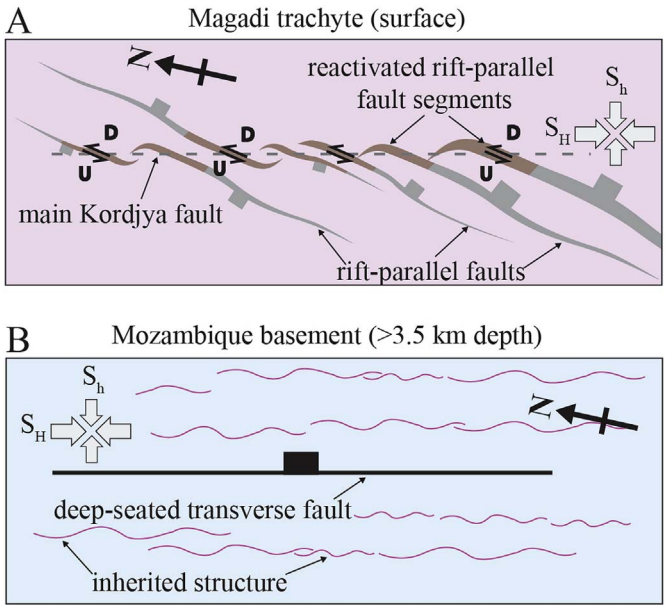

Fig. 12. Conceptual model of the kinematics of the Kordjya fault system in the (A) near-surface and (B) at basement depths. The regional stress field is indicated by the orientation of the maximum (S_H) and minimum compressive stress directions (S_h). A: Map view illustration of fault mechanics of the Kordjya fault within Magadi trachyte lavas in the near-surface. Rift-parallel faults (grey polygons) trending oblique to the trace of the main Kordjya fault (dashed grey line) are preferentially reactivated in the vicinity of the Kordjya fault (light brown fault segments) as sinistral-oblique-normal faults in order to accommodate dip-slip motion along a NNW-trending normal fault at basement depths (B). Half-arrows show the sense of horizontal shear of the rift-parallel faults, whereas D and U correspond to the down-thrown hanging walls and up-thrown footwalls, respectively, in response to dip-slip displacements at depth. B: Within the Proterozoic basement, the Kordjya fault is interpreted in this study to behave as a pure dip-slip normal fault through the reactivation of a NNW-trending, transverse, inherited structure of the Aswa shear zone. The depth of basement (> 3.5 km) is based on the thickness of rift-basin sediments and volcanics from Birt et al. (1997). (For interpretation of the references to colour in this figure legend, the reader is referred to the web version of this article.)

2017) and northern portion of the Nguruman border fault. Similar counter-clockwise rotations of σ_3 is inferred for NNW-trending transverse faults and volcanic cone lineaments between the left-stepping Pangani and Natron basins further south (Tanzania) (Muirhead et al., 2015). Additionally, the newly developing magmatic segment below the Lake Magadi region (Weinstein et al., 2017) may have loaded the crust and induced flexure of the rift floor (Corti et al., 2015), potentially contributing to the observed local stress rotation (e.g., Cailleau et al., 2003).

These observations show that transverse faults exploiting pre-existing weaknesses, like the Kordjya fault, may initiate at later stages of rift basin evolution and act as critical kinematic linkages between developing centers of magmatic and tectonic strain. Although additional NNW-trending transverse faults are present in the Magadi rift basin (Fig. 1C), the Kordjya fault is unique in that it has accumulated a large amount of throw (> 300 m) and directly links with the Lengitoto border fault segment. These observations suggests that: (1) this structure has become the dominant transverse feature within the Magadi basin; and (2) slip along the Kordjya fault has become the preferred mode of strain transfer from the rift border to the rift center.

The preference for fault slip along the Kordjya fault, rather than other transverse features, may, in part, relate to the presence of an influential basement weakness and, potentially, magmatic volatile release in this part of rift. In support of the former, the Kordjya fault has localized along the same NNW-trending, transverse structural zone as the Lengitoto border fault segment. Both of these faults line up along the NNW-striking Engorika-Magadi-Lembolos lineament of Smith and Mosley (1993) (Fig. 1B), which is a transverse structural fabric that has developed within the Aswa shear zone (Fig. 1A). During the initial stages of rifting in Magadi, which were characterized by border fault development, this basement weakness also acted as a locus of strain transfer, accommodating a left-step in the rift-bounding fault system (i.e., Smith and Mosley, 1993) (Fig. 11B). Observations presented here suggest that this basement weakness continues to play a role in strain transfer in the present day. We interpret that the Kordjya fault represents an extension of the original Lengitoto fault segment, where both these structures currently act as two kinematically coherent fault segments, thereby connecting the newly developed locus of strain in the rift center with the older locus of strain along the rift border. By transferring strain to the rift center, the Kordjya fault may be creating a progressive bypass of strain accommodation along the Nguruman fault south of the Lengitoto segment (Fig. 13C).

The preference for fault slip along the transverse Kordjya fault may have been further assisted by the rise of magmatic fluids within the rift center. Although spring systems situated near Lake Magadi typically rise to the surface along rift-parallel faults, they also emanate from the Kordjya fault along a ~10 km stretch at the southeastern end of the structure (Fig. 6). Carbon and helium isotope data of springs and diffuse soil CO_2 flux data (Lee et al., 2016, 2017; Muirhead et al., 2016) also support the rise of significant volumes of magmatic volatiles along the NNW-striking Kordjya fault. Fluid infiltration is shown to weaken faults from hydration mineral reactions (Moore and Rymer, 2007) and enhanced pore-fluid pressures (Sibson, 2000); thus, magmatic volatile release associated with the migrating locus of magmatic activity at depth (Weinstein et al., 2017) (Fig. 13C) could feasibly have assisted in the development of the transverse Kordjya fault in this part of the rift.

Although this study is unable to quantify the extent to which faulting along the Kordjya fault has been assisted by fault-fluid interactions, the idea is consistent with transfer zones in continental rifts elsewhere. For example, transfer faults in the Taupo Rift (New Zealand) produce zones of increased vertical permeability where they intersect rift-parallel faults (Rowland and Simmons, 2012). Factors like this contribute to higher bulk permeabilities in transfer zones compared to rift segments, resulting in enhanced hydrothermal fluid flow (Rowland and Sibson, 2004; Wilson and Rowland, 2016). These zones are prone to fluid-assisted failure, with fault weakening driven by changes in pore-fluid pressure (Rowland and Simmons, 2012). It is therefore possible that the release of magmatic fluids along the Kordjya fault system—in addition to the effects of inherited basement weaknesses—assisted faulting along this part of the Magadi basin, promoting development of a major transfer fault structure.

5. Conclusions

This study provides a revised field and remote-sensing analysis of the mechanics of faulting along the transverse Kordjya fault of the Magadi basin in order to ascertain the role of transverse faulting in rift evolution. Our analysis demonstrates that the NNW-trending, transverse Kordjya fault is a complex system of inherited and reactivated NNE-striking, left-stepping, en echelon, rift-parallel normal faults. The structure developed by reactivating the rift-parallel normal faults as oblique-normal faults with a component of sinistral shear. These kinematically coherent oblique-normal faults collectively accommodate dip-slip motion along a reactivated, underlying, NNW-trending basement structure likely related to the Aswa shear zone.

Field analysis of tectonic joint sets and fault slip vectors also show that the least compressive stress in the vicinity of the Kordjya fault rotated to an ENE-WSW direction, in contrast to the ESE-WNW regional extension direction throughout the remainder of the basin. The tendency for predominantly dip-slip fault activity along transverse features suggests a recent change in rift driving forces in the Magadi basin. These changes are likely the result of an interplay among magma-assisted strain localization at the rift center, inherited crustal fabrics, and a localized counter-clockwise rotation of σ_3 related to interacting

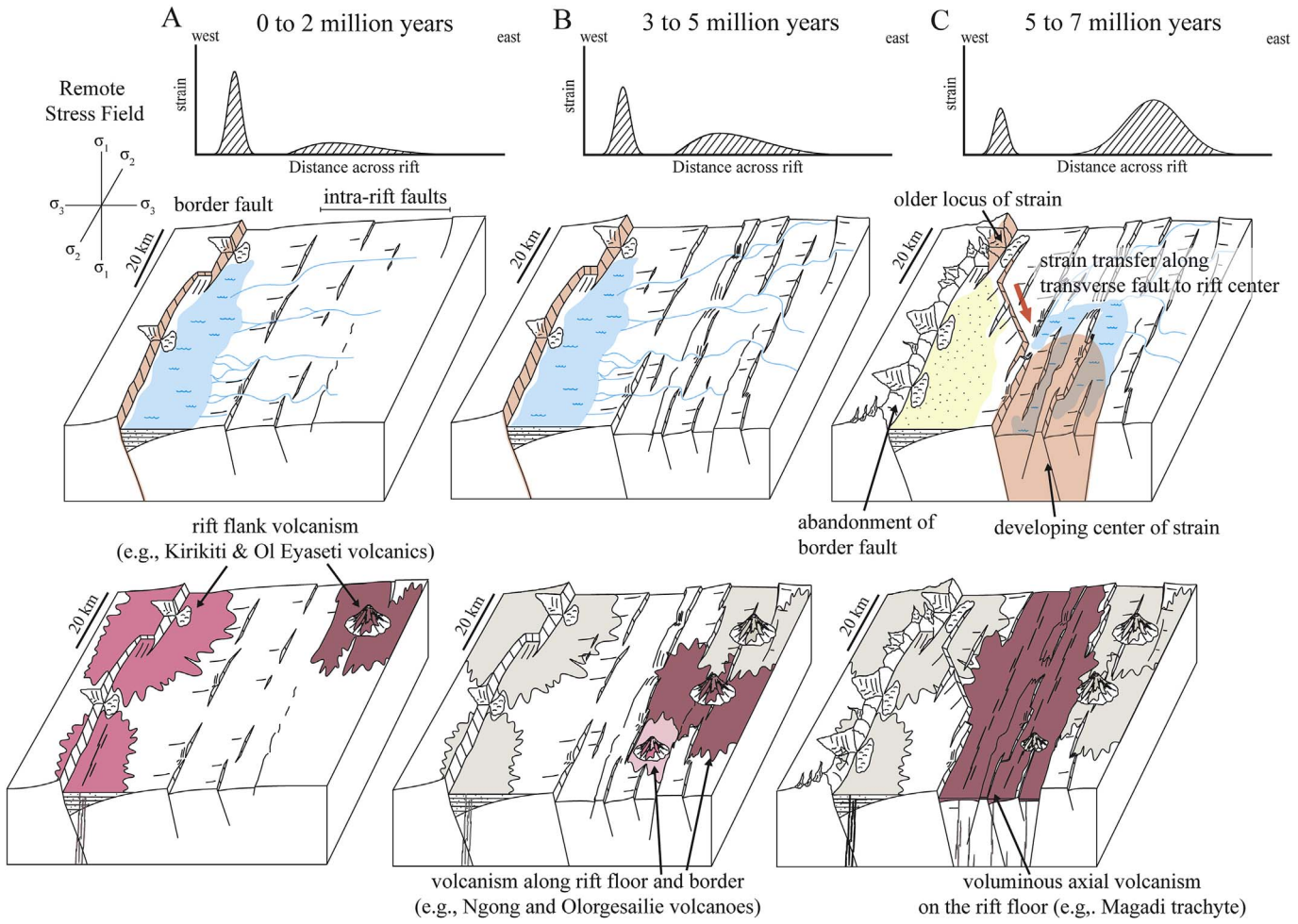

Fig. 13. Conceptual model of the tectonic-magmatic evolution of the Magadi basin and the development of the transverse Kordjya fault. In parts A-C, the top panel shows the distribution of fault strain (idealized graphs) across the rift and through Lake Magadi based on existing models of basin evolution in the Eastern rift branch (e.g., Ebinger, 2005) and fault system analyses from Muirhead et al. (2016), the middle panel shows the corresponding conceptual rift basin tectonic architecture (areas of high fault strain highlighted pink), and the bottom panel shows the (idealized) distribution of volcanic activity. A: During the earliest stages of rifting (first 2 million years), upper crustal strain is focused on the western border of the basin, and volcanism occurs on the eastern and western boundaries (lavas shown in pink and brown). B: 2–5 million years after rift initiation. Strain is primarily accommodated along the rift borders; however, a system of intra-rift faults begins to develop. Volcanism occurs along both the rift borders and the central rift axis. C: In the past few million years of rifting, fault strain became focused into the center of the Magadi basin below Lake Magadi. Geophysical data suggest that the migration of fault strain is in response to a developing magmatic segment beneath the rift (Roecker et al., 2017; Weinstein et al., 2017), which is supported by the release of magmatic volatiles in the rift center (Lee et al., 2016, 2017). The transverse Kordjya fault developed in response to the changing rift basin architecture and kinematically links the center of the basin with older locus of strain along the Lengitoto segment of the border fault system. (For interpretation of the references to colour in this figure legend, the reader is referred to the web version of this article.)

segments of the southern Kenya Rift. Since the Mid-to Late Pleistocene, the Kordjya fault has become a dominant transverse feature within the rift basin, and represents a southeastern extension of the original Lengitoto border fault segment. This fault currently acts as a critical kinematic linkage between the newly developed locus of strain in the rift center and the older locus of strain along the rift border fault. The preference for fault slip along the Kordjya fault, rather than other transverse structures, may relate to the presence of an influential basement weakness and a contribution from fault-weakening by magmatic fluids. By assisting in the transfer of strain to the rift center, the Kordjya fault effectively acts to cut off the Nguruman border fault south of the Lengitoto segment.

In summary, the results from this study have implications for the timing and kinematics of fault systems that exploit preexisting basement weaknesses in the EARS. Specifically, field observations and data from this study lead to the following broad conclusions:

1) During rift development, preexisting transverse structures in basement rocks can be reactivated in response to evolving magmatic systems and basin tectonic architecture.
2) The reactivation of these preexisting weaknesses and subsequent formation of transverse faults can postdate the development of widespread rift-parallel fault systems within rift basins.
3) Reactivated basement structures may cannibalize this inherited structure in overlying, young basement-fill volcanics in order to develop a through-going transverse structure at the surface.
4) Transverse faults throughout the EARS may exhibit predominantly dip-slip kinematics due to local rotations of σ_3.
5) Transverse structures such as the Kordjya fault may assist in the progressive transfer of the locus of strain accommodation from the rift border fault system toward the rift center. This transfer is concomitant with the migration of the underlying magmatic system toward the rift center, creating a voluminous flow of volatiles that may assist in transverse fault development.

It follows that recently activated transverse faults observed throughout the EARS may not only reveal the effects of inherited basement weaknesses on fault system dynamics, but also provide important clues regarding developing magmatic and tectonic stain fields as continental rift basins evolve.

Acknowledgements

Fieldwork and writing of this study was supported by National Science Foundation grants EAR-1113677 (to Kattenhorn) and EAR-1654518 (Muirhead). Additional support to Muirhead was provided by Fulbright New Zealand and the Ministry of Science and Innovation during his PhD research. We thank the Kenyan National Council for Science and Technology for granting research permits, and Norbert Opiyo-Akech for assistance. Aerial photographs were provided by the Polar Geospatial Center, University of Minnesota (St. Paul). We thank Cindy Ebinger in particular for valuable discussions on continental rifting, and Eric Mittelstaedt, Catherine Cooper, John Watkinson, Dennis Geist, and Alexa Van Eaton for helpful discussions and comments. We are grateful to Gladys Kianji and Edwin Dindi for assistance in the field. Reviewer Giacomo Corti and an anonymous reviewer provided helpful and constructive critiques of an earlier version of this manuscript.

References

Acosta, V.T., Bande, A., Sobel, E.R., Parra, M., Schildgen, T.F., Stuart, F., Strecker, M.R., 2015. Cenozoic extension in the Kenya Rift from low-temperature thermochronology: links to diachronous spatiotemporal evolution of rifting in East Africa. Tectonics 34, 2367–2386.

Agostini, A., Corti, G., Zeoli, A., Mulugeta, G., 2009. Evolution, pattern, and partitioning of deformation during oblique continental rifting: inferences from lithospheric-scale centrifuge models. Geochem. Geophys. Geosyst. 10. http://dx.doi.org/10.1029/2009GC002676.

Agostini, A., Bonini, M., Corti, G., Sani, F., Mazzarini, F., 2011. Fault architecture in the Main Ethiopian Rift and comparison with experimental models: implications for rift evolution and Nubia–Somalia kinematics. Earth Planet. Sci. Lett. 301, 479–492.

Allken, V., Huismans, R.S., Thieulot, C., 2011. Three-dimensional numerical modeling of upper crustal extensional systems. J. Geophys. Res. 116. http://dx.doi.org/10.1029/2011JB008319.

Anderson, E.M., 1951. The Dynamics of Faulting and Dyke Formation with Applications to Britain. Oliver and Boyd, Edinburgh, pp. 206.

Angelier, J., Bergerat, F., Dauteuil, O., Villemin, T., 1997. Effective tension-shear relationships in extensional fissure swarms, axial rift zone of northeastern Iceland. J. Struct. Geol. 19, 673–685.

Atmaoui, N., Hollnack, D., 2003. Neotectonics and extension direction of the southern Kenya Rift, Lake Magadi area. Tectonophysics 364, 71–83.

Baker, B.H., 1958. Geology of the Magadi Area. pp. 81 Geological Survey of Kenya.

Baker, B.H., 1963. Geology of the Area of South of Magadi. pp. 27 Geological Survey of Kenya.

Baker, B.H., Wohlenberg, J., 1971. Structure and evolution of Kenya rift valley. Nature 229, 538–542.

Baker, B.H., Mitchell, J.G., 1976. Volcanic stratigraphy and geochronology of the Kedong-Olorgesaile area and the evolution of the south Kenya rift valley. J. Geol. Soc. Lond. 132, 467–484.

Baker, B.H., Williams, L.A., Miller, J.A., Fitch, F.J., 1971. Sequence and geochronology of Kenya Rift volcanics. Tectonophysics 11, 191–215.

Behr, H.J., Röhricht, C., 2000. Record of seismotectonic events in siliceous cyanobacterial sediments (Magadi cherts), Lake Magadi, Kenya. Int. J. Earth Sci. 89, 268–283.

Ben-Avraham, Z., Ten Brink, U., 1989. Transverse faults and segmentation of basins within the dead sear rift. J. Afr. Earth Sci. 8, 603–616.

Berryman, K., Villamor, P., Nairn, I., van Dissen, R., Begg, J., Lee, J., 2008. Late Pleistocene surface rupture history of the Paeroa fault, Taupo rift, New Zealand. N. Z. J. Geol. Geophys. 51, 135–158.

Beutel, E., van Wijk, J., Ebinger, C., Keir, D., Agostini, A., 2010. Formation and stability of magmatic segments in the Main Ethiopian and Afar rifts. Earth Planet. Sci. Lett. 293, 225–235.

Bialas, R.W., Buck, W.R., Qin, R., 2010. How much magma is required to rift a continent? Earth Planet. Sci. Lett. 292, 68–78.

Birt, C.S., Maguire, P.K.H., Khan, M.A., Thybo, H., Keller, G.R., Patel, J., 1997. The influence of pre-existing structures on the evolution of the southern Kenya Rift Valley - evidence from seismic and gravity studies. Tectonophysics 278, 211–242.

Bott, M.H.P., 1996. Flexure associated with planar faulting. Geophys. J. Int. 126. http://dx.doi.org/10.1111/j.1365-246X.1996.tb04692.x.

Buck, W.R., 2004. Consequences of asthenospheric variability on continental rifting. In: Karner, G.D. (Ed.), Rheology and Deformation of the Lithosphere at Continental Margins: MARGINS Theoretical and Experimental Earth Science Series. Columbia University Press, New York, pp. 1–30.

Buck, W.R., 2006. The role of magma in the development of the Afro-Arabian Rift System. Geol. Soc. Lond. Special Publ. 259, 43–54.

Brune, S., 2014. Evolution of stress and fault patterns in oblique rift systems: 3-D numerical lithospheric-scale experiments from rift to breakup. Geochem. Geophys. Geosyst. 15, 3392–3415.

Cailleau, B., Walter, T.R., Janle, P., Hauber, E., 2003. Modeling volcanic deformation in a regional stress field: implications for the formation of graben structures on Alba Patera, Mars. J. Geophys. Res. Planets 108. http://dx.doi.org/10.1029/2003JE002135.

Calais, E., d'Oreye, N., Albaric, J., Deschamps, A., Delvaux, D., Deverchere, J., Ebinger, C., Ferdinand, R.W., Kervyn, F., Macheyeki, A.S., Oyen, A., Perrot, J., Saria, E., Smets, B., Stamps, D.S., Wauthier, C., 2008. Strain accommodation by slow slip and dyking in a youthful continental rift, East Africa. Nature 456, 783–788.

Cartwright, J.A., Trudgill, B.D., Mansfield, C.S., 1995. Fault growth by segment linkage - an explanation for scatter in maximum displacement and trace length data from the Canyonlands grabens of SE Utah. J. Struct. Geol. 17, 1319–1326.

Childs, C., Nicol, A., Walsh, J.J., Watterson, J., 1996. Growth of vertically segmented normal faults. J. Struct. Geol. 18, 1389–1397.

Chorowicz, J., 1989. Transfer and transform fault zones in continental rifts: examples in the Afro-Arabian Rift System. Implications of crust breaking. J. Afr. Earth Sci. 8, 203–214.

Chorowicz, J., 1992. The role of ancient structures in the genesis and evolution of the East African Rift. Bull. De. La Soc. Geol. De. Fr. 163, 217–227.

Chorowicz, J., Sorlien, C., 1992. Oblique extensional tectonics in the Malawi rift, Africa. Geol. Soc. Am. Bull. 104, 1015–1023.

Corti, G., van Wijk, J., Cloetingh, S., Morley, C.K., 2007. Tectonic inheritance and continental rift architecture: numerical and analogue models of the East African Rift system. Tectonics 26. http://dx.doi.org/10.1029/2006TC002086.

Corti, G., 2008. Control of rift obliquity on the evolution and segmentation of the main Ethiopian rift. Nat. Geosci. 1, 258–262.

Corti, G., 2009. Continental rift evolution: from rift initiation to incipient break-up in the Main Ethiopian Rift, East Africa. Earth Sci. Rev. 96, 1–53.

Corti, G., 2012. Evolution and characteristics of continental rifting: analog modeling-inspired view and comparison with examples from the East African Rift System. Tectonophysics 522, 1–33.

Corti, G., Philippon, M., Sani, F., Keir, D., Kidane, T., 2013. Re-orientation of the extension direction and pure extensional faulting at oblique rift margins: comparison between the Main Ethiopian Rift and laboratory experiments. Terra Nova 25, 396–404.

Corti, G., Agostini, A., Keir, D., Van Wijk, J., Bastow, I.D., Ranalli, G., 2015. Magma-induced axial subsidence during final-stage rifting: implications for the development of seaward-dipping reflectors. Geosphere 11, 563–571.

Crossley, R., 1979. The Cenozoic stratigraphy and structure of the western part of the Rift Valley in southern Kenya. J. Geol. Soc. Lond. 136, 393–405.

Cruikshank, K.M., Zhao, G.H., Johnson, A.M., 1991. Analysis of minor fractures associated associated with joints and faulted joints. J. Struct. Geol. 13, 865–886.

Daly, M.C., Chorowicz, J., Fairhead, J.D., 1989. Rift basin evolution in Africa: the influence of steep basement shear zones. Geol. Soc. Lond. Special Publ. 44, 309–334.

Daniels, K.A., Bastow, I.D., Keir, D., Sparks, R.S.J., Menand, T., 2014. Thermal models of dyke intrusion during development of continent-ocean transition. Earth Planet. Sci. Lett. 385, 145–153.

Dawers, N.H., Anders, M.H., Scholz, C.H., 1993. Growths of normal faults - displacement-length scaling. Geology 21, 1107–1110.

Delvaux, D., 2001. Tectonic and palaeostress evolution of the Tanganyika-Rukwa-Malawi rift segment, East African rift system. In: Peri-tethys Memoir 6: Peri-tethyan Rift/Wrench Basins and Passive Margins, vol. 186. pp. 545–566.

Delvaux, D., Barth, A., 2010. African stress pattern from formal inversion of focal mechanism data. Tectonophysics 482, 105–128.

Delvaux, D., Levi, K., Kajara, R., Sarota, J., 1992. Cenozoic paleostress and kinematic evolution of the Rukwa: north Malawi rift valley (East African Rift System). Bull. Des. Centres De. Rech. Explor. Prod. Elf Aquitaine 16, 383–406.

Delvaux, D., Kervyn, F., Macheyeki, A.S., Temu, E.B., 2012. Geodynamic significance of the TRM segment in the East African rift (W-Tanzania): active tectonics and paleostress in the Ufipa plateau and Rukwa basin. J. Struct. Geol. 37, 161–180.

DeMets, C., Merkouriev, S., 2016. High-resolution estimates of Nubia–Somalia plate motion since 20 Ma from reconstructions of the southwest indian ridge, red sea and Gulf of aden. Geophys. J. Int. 207, 317–332.

Densmore, A.L., Gupta, S., Allen, P.A., Dawers, N.H., 2007. Transient landscapes at fault tips. J. Geophys. Res.Earth Surf. 112. http://dx.doi.org/10.1029/2006JF000560.

Dixon, T.H., Stern, R.J., Hussein, I.M., 1987. Control of red sea rift geometry by precambrian structures. Tectonics 6, 551–571.

Downs, D.T., Rowland, J.V., Wilson, C.J.N., Rosenberg, M.D., Leonard, G.S., Calvert, A.T., 2014. Evolution of the intra-arc Taupo-Reporoa basin within the Taupo volcanic zone of New Zealand. Geosphere 10, 185–206.

Dunbar, J.A., Sawyer, D.S., 1989. How preexisting weaknesses control the style of continental breakup. J. Geophys. Res. 94. http://dx.doi.org/10.1029/JB094iB06p07278.

Ebinger, C.J., 1989. Geometric and kinematic development of border faults and accommodation zones, Kivu-Rusizi Rift, Africa. Tectonics 8, 117–133.

Ebinger, C., 2005. Continental break-up: the East African perspective. Astron. Geophys. 46, 16–21.

Ebinger, C.J., Casey, M., 2001. Continental breakup in magmatic provinces: an Ethiopian example. Geology 29, 527–530.

Ebinger, C., Scholz, C.A., 2012. Continental rift basins: the East African perspective. In: Tectonics of Sedimentary Basins: Recent Advances, pp. 185–208.

Ebinger, C.J., Karner, G.D., Weissel, J.K., 1991. Mechanical strength of extended continental lithosphere: constraints from the Western rift system, East Africa. Tectonics 10, 1239–1256.

Ebinger, C.J., Yemane, T., Harding, D.J., Tesfaye, S., Kelley, S., Rex, D.C., 2000. Rift deflection, migration, and propagation: linkage of the Ethiopian and Eastern rifts, Africa. Geol. Soc. Am. Bull. 112, 163–176.

Ebinger, C.J., van Wijk, J., Keir, D., 2013. The time scales of continental rifting: implications for global processes. In: Bickford, M.E. (Ed.), The Web of Geological Sciences: Advances, Impacts, and Interactions, pp. 1–26 Geological Society of America Special Paper 500.

Foster, A., Ebinger, C., Mbede, E., Rex, D., 1997. Tectonic development of the northern Tanzanian sector of the East African rift system. J. Geol. Soc. Lond. 154, 689–700.
Galadini, F., Galli, P., 2000. Active tectonics in the central Apennines (Italy) - input data for seismic hazard assessment. Nat. Hazards 22, 225–270.
Gibbs, A.D., 1984. Structural evolution of extensional basin margins. J. Geol. Soc. 141, 609–620.
Grant, J.V., Kattenhorn, S.A., 2004. Evolution of vertical faults at an extensional plate boundary, southwest Iceland. J. Struct. Geol. 26, 537–557.
Gudmundsson, A., 1992. Formation and growth of normal faults at the divergent plate boundary in Iceland. Terra Nova 4, 464–471.
Guth, A.L., 2015. Volcanic volumes associated with the Kenya Rift: recognition and correlation of preservation biases. Geol. Soc. Lond. Special Publ. 420, 43–67.
Hetzel, R., Strecker, M.R., 1994. Late Mozambique Belt structures in western Kenya and their influence on the evolution of the Cenozoic Kenya Rift. J. Struct. Geol. 16, 189–201.
Hetzel, R., Hampel, A., 2005. Slip rate variations on normal faults during glacial-interglacial changes in surface loads. Nature 435, 81–84.
Hui, H., Peslier, A.H., Rudnick, R.L., Simonetti, A., Neal, C.R., 2015. Plume-cratonic lithosphere interaction recorded by water and other trace elements in peridotite xenoliths from the Labait volcano, Tanzania. Geochem. Geophys. Geosyst. 16. http://dx.doi.org/10.1002/2015GC005779.
Iaffaldano, G., Hawkins, R., Sambridge, M., 2014. Bayesian noise-reduction in Arabia/Somalia and Nubia/Arabia finite rotations since ~ 20 Ma: implications for Nubia/Somalia relative motion. Geochem. Geophys. Geosyst. 15, 845–854.
Ibs-von Seht, M., Blumenstein, S., Wagner, R., Hollnack, D., Wohlenberg, J., 2001. Seismicity, seismotectonics and crustal structure of the southern Kenya Rift - new data from the Lake Magadi area. Geophys. J. Int. 146, 439–453.
Kattenhorn, S.A., 2004. Strike-slip fault evolution on Europa: evidence from tailcrack geometries. Icarus 172, 582–602.
Kattenhorn, S.A., Krantz, B., Walker, E.L., Blakeslee, M.W., 2016. Evolution of the Hat Creek fault system, northern California. In: Krantz, B., Ormand, C., Freeman, B. (Eds.), 3-D Structural Interpretation: Earth, Mind, and Machine. AAPG Memoir, vol. 111. pp. 121–154.
Katumwehe, A.B., Abdelsalam, M.G., Atekwana, E.A., 2015a. The role of pre-existing Precambrian structures in rift evolution: the Albertine and Rhino grabens, Uganda. Tectonophysics 646, 117–129.
Katumwehe, A.B., Abdelsalam, M.G., Atekwana, E.A., Laó-Dávila, D.A., 2015b. Extent, kinematics and tectonic origin of the precambrian Aswa shear zone in eastern Africa. Gondwana Res. 34, 241–253.
Keir, D., Ebinger, C.J., Stuart, G.W., Daly, E., Ayele, A., 2006. Strain accommodation by magmatism and faulting as rifting proceeds to breakup: seismicity of the northern Ethiopian rift. J. Geophys. Res. Solid Earth 111. http://dx.doi.org/10.1029/2005jb003748.
Kendall, J.M., Stuart, G.W., Ebinger, C.J., Bastow, I.D., Keir, D., 2005. Magma-assisted rifting in Ethiopia. Nature 433, 146–148.
Kent, G.M., Babcock, J.M., Driscoll, N.W., Harding, A.J., Dingler, J.A., Seitz, G.G., Gardner, J.V., Mayer, L.A., Goldman, C.R., Heyvaert, A.C., Richards, R.C., Karlin, R., Morgan, C.W., Gayes, P.T., Owen, L.A., 2005. 60 k.y. record of extension across the western boundary of the Basin and Range province: estimate of slip rates from offset shoreline terraces and a catastrophic slide beneath Lake Tahoe. Geology 33, 365–368.
Keranen, K., Klemperer, S.L., 2008. Discontinuous and diachronous evolution of the Main Ethiopian Rift: implications for development of continental rifts. Earth Planet. Sci. Lett. 265, 96–111.
Kilembe, E.A., Rosendahl, B.R., 1992. Structure and stratigraphy of the Rukwa rift. Tectonophysics 209, 143–158.
Kinabo, B.D., Hogan, J.P., Atekwana, E.A., Abdelsalam, M.G., Modisi, M.P., 2008. Fault growth and propagation during incipient continental rifting: insights from a combined aeromagnetic and Shuttle Radar Topography Mission digital elevation model investigation of the Okavango Rift Zone, northwest Botswana. Tectonics 27. http://dx.doi.org/10.1029/2007TC002154.
Koehn, D., Aanyu, K., Haines, S., Sachau, T., 2008. Rift nucleation, rift propagation and the creation of basement micro-plates within active rifts. Tectonophysics 458, 105–116.
Koehn, D., Lindenfeld, M., Rumpker, G., Aanyu, K., Haines, S., Passchier, C.W., Sachau, T., 2010. Active transsection faults in rift transfer zones: evidence for complex stress fields and implications for crustal fragmentation processes in the western branch of the East African Rift. Int. J. Earth Sci. 99, 1633–1642.
Koptev, A., Calais, E., Burov, E., Leroy, S., Gerya, T., 2015. Dual continental rift systems generated by plume–lithosphere interaction. Nat. Geosci. 8, 388–392.
Kolawole, F., Atekwana, E.A., Malloy, S., Stamps, D.S., Grandin, R., Abdelsalam, M.G., Leseane, K., Shemang, E.M., 2017. Aeromagnetic, gravity, and differential interferometric synthetic aperture radar analyses reveal the causative fault of the 3 April 2017 Mw 6.5 moiyabana, Botswana, earthquake. Geophys. Res. Lett. 44. http://dx.doi.org/10.1002/2017GL074620.
Laó-Dávila, D.A., Al-Salmi, H.S., Abdelsalam, M.G., Atekwana, E.A., 2015. Hierarchical segmentation of the Malawi Rift: the influence of inherited lithospheric heterogeneity and kinematics in the evolution of continental rifts. Tectonics 34, 2399–2417.
Lee, H., Muirhead, J.D., Fischer, T.P., Ebinger, C.J., Kattenhorn, S.A., Sharp, Z.D., Kianji, G., 2016. Massive and prolonged deep carbon emissions associated with continental rifting. Nat. Geosci. 9, 145–149.
Lee, H., Fischer, T.P., Muirhead, J.D., Ebinger, C.J., Kattenhorn, S.A., Sharp, Z.D., Kianji, G., Takahata, N., Sano, Y., 2017. Incipient rifting accompanied by the release of subcontinental lithospheric mantle volatiles in the Magadi and Natron basin, East Africa. J. Volcanol. Geotherm. Res. http://dx.doi.org/10.1016/j.jvolgeores.2017.03.017.
Le Gall, B., Tiercelin, J.J., Richert, J.P., Gente, P., Sturchio, N.C., Stead, D., Le Turdu, C., 2000. A morphotectonic study of an extensional fault zone in a magma-rich rift: the Baringo Trachyte Fault System, central Kenya Rift. Tectonophysics 320, 87–106.
Le Gall, B., Nonnotte, P., Rolet, J., Benoit, M., Guillou, H., Mousseau-Nonnotte, M., Albaric, J., Deverchere, J., 2008. Rift propagation at craton margin. Distribution of faulting and volcanism in the north Tanzanian divergence (East Africa) during Neogene times. Tectonophysics 448, 1–19.
Le Turdu, C., Richert, J.P., Xavier, J.-P., Renaut, R.W., Tiercelin, J.-J., Rolet, J., Lezzar, K.E., Coussement, C., 1999. Influence of preexisting oblique discontinuities on the geometry and evolution of extensional fault patterns: evidence from the Kenya Rift using SPOT imagery. In: Morley, C.K. (Ed.), Geoscience of Rift Systems – Evolution of East Africa. American Association of Petroleum Geologists, Tulsa, OK, USA, pp. 173–191.
Leseane, K., Atekwana, E.A., Mickus, K.L., Abdelsalam, M.G., Shemang, E.M., Atekwana, E.A., 2015. Thermal perturbations beneath the incipient Okavango rift zone, northwest Botswana. J. Geophys. Res. Solid Earth 120, 1210–1228.
Lithgow-Bertelloni, C., Guynn, J.H., 2004. Origin of the lithospheric stress field. J. Geophys. Res. 109. http://dx.doi.org/10.1029/2003JB002467.
Machette, M.N., Personius, S.F., Nelson, A.R., 1991. The Wasatch fault zone, Utah - segmentation and history of Holocene earthquakes. J. Struct. Geol. 13, 137–149.
Mana, S., Furman, T., Turrin, B.D., Feigenson, M.D., Swisher, C.C., 2015. Magmatic activity across the East African north Tanzanian divergence zone. J. Geol. Soc. 172, 368–389.
Manighetti, I., King, G.C.P., Gaudemer, Y., Scholz, C.H., Doubre, C., 2001. Slip accumulation and lateral propagation of active normal faults in Afar. J. Geophys. Res. Solid Earth 106, 13667–13696.
Marshall, S.T., Kattenhorn, S.A., 2005. A revised model for cycloid growth mechanics on Europa: evidence from surface morphologies and geometries. Icarus 177, 341–366.
Modisi, M.P., Atekwana, E.A., Kampunzu, A.B., Ngwisanyi, T.H., 2000. Rift kinematics during the incipient stages of continental extension: evidence from the nascent Okavango rift basin, northwest Botswana. Geology 28, 939–942.
Moore, D.E., Rymer, M.J., 2007. Talc-bearing serpentinite and the creeping section of the San Andreas fault. Nature 448, 795–797.
Morley, C.K., Nelson, R.A., Patton, T.L., Munn, S.G., 1990. Transfer zones in the East African rift system and their relevance to hydrocarbon exploration in rifts. AAPG Bull. 74, 1234–1253.
Morley, C.K., 1995. Developments in the structural geology of rifts over the last decade and their impact on hydrocarbon exploration. Hydrocarbon Habitat Rift Basins 1–32.
Morley, C.K., 2010. Stress re-orientation along zones of weak fabrics in rifts: an explanation for pure extension in 'oblique' rift segments? Earth Planet. Sci. Lett. 297, 667–673.
Morley, C.K., Wescott, W.A., Stone, D.M., Harper, R.M., Wigger, S.T., Karanja, F.M., 1992. Tectonic evolution of the northern Kenya Rift. J. Geol. Soc. 149, 333–348.
Morley, C.K., Haranya, C., Phoosongsee, W., Pongwapee, S., Kornsawan, A., Wonganan, N., 2004. Activation of rift oblique and rift parallel pre-existing fabrics during extension and their effect on deformation style: examples from the rifts of Thailand. J. Struct. Geol. 26, 1803–1829.
Mosley, P.N., 1993. Geological evolution of the late proterozoic Mozambique Belt of Kenya. Tectonophysics 221, 223–250.
Muirhead, J.D., Kattenhorn, S.A., Le Corvec, N., 2015. Varying styles of magmatic strain accommodation across the East African Rift. Geochem. Geophys. Geosyst. 16, 2775–2795.
Muirhead, J.D., Kattenhorn, S.A., Lee, H., Mana, S., Turrin, B.D., Fischer, T.P., Kianji, G., Dindi, E., Stamps, D.S., 2016. Evolution of upper crustal faulting assisted by magmatic volatile release during early-stage continental rift development in the East African Rift. Geosphere 12, 1670–1700.
Nicol, A., Watterson, J., Walsh, J.J., Childs, C., 1996. The shapes, major axis orientations and displacement patterns of fault surfaces. J. Struct. Geol. 18, 235–248.
Nyamai, C.M., Mathu, E.M., Opiyo-Akech, N., Wallbrecher, E., 2003. A reappraisal of the geology, geochemistry, structures and tectonics of the Mozambique Belt in Kenya, east of the rift system. Afr. J. Sci. Technol. 4, 51–71.
Philippon, M., Willingshofer, E., Sokoutis, D., Corti, G., Sani, F., Bonini, M., Cloetingh, S., 2015. Slip re-orientation in oblique rifts. Geology 43, 147–150.
Pollard, D.D., Aydin, A., 1984. Propagation and linkage of oceanic ridge segments. J. Geophys. Res. 89, 10017–10028.
Pollard, D.D., Aydin, A., 1988. Progress in understanding jointing over the past century. Geol. Soc. Am. Bull. 100, 1181–1204.
Ring, U., 1994. The influence of preexisting structure on the evolution of the Cenozoic Malawi rift (East African rift system). Tectonics 13, 313–326.
Ring, U., Betzler, C., Delvaux, D., 1992. Normal vs strike-slip faulting during development in East Africa: the Malawi Rift. Geology 20, 1015–1018.
Ring, U., Schwartz, H.L., Bromage, T.G., Sanaane, C., 2005. Kinematic and sedimentological evolution of the manyara rift in northern Tanzania, East Africa. Geol. Mag. 142, 355–368.
Robertson, E.A.M., Biggs, J., Cashman, K.V., Floyd, M.A., Vye-Brown, C., 2015. Influence of regional tectonics and pre-existing structures on the formation of elliptical calderas in the Kenyan Rift. Geol. Soc. Lond. Spec. Publ. 420, 43–67.
Rodríguez, E., Morris, C.S., Belz, J.E., Chapin, E.C., Martin, J.M., Daffer, W., Hensley, S., 2005. An Assessment of the SRTM Topographic Products. pp. 125 Jet Propulsion Laboratory Technical Report D-31639.
Roecker, S., Ebinger, C., Tiberi, C., Mulibo, G., Ferdinand-Wambura, R., Mtelela, K., Kianji, G., Muzuka, A., Gautier, S., Albaric, J., Peyrat, S., 2017. Subsurface images of the Eastern Rift, Africa, from the joint inversion of body waves, surface waves and gravity: investigating the role of fluids in early-stage continental rifting. Geophys. J. Int. 210, 931–950.
Rosendahl, B.R., 1987. Architecture of continental rifts with special reference to East Africa. Annu. Rev. Earth Planet. Sci. 15, 445–503.

Rowland, J.V., Sibson, R.H., 2004. Structural controls on hydrothermal flow in a segmented rift system, Taupo Volcanic Zone, New Zealand. Geofluids 4, 259–283.
Rowland, J.V., Simmons, S.F., 2012. Hydrologic, magmatic, and tectonic controls on hydrothermal flow, Taupo volcanic zone, New Zealand: implications for the formation of epithermal vein deposits. Econ. Geol. 107, 427–457.
Saggerson, E.P., 1991. Geology of the Nairobi Area. Geological Survey of Kenya Report 98. Mines and Geological Department, Nairobi, Kenya, pp. 91.
San'kov, V., Deverchere, J., Gaudemer, Y., Houdry, F., Filippov, A., 2000. Geometry and rate of faulting in the north Baikal rift, siberia. Tectonics 19, 707–722.
San'kov, V.A., Lukhnev, A.V., Miroshnichenko, A.I., Ashurkov, S.V., Byzov, L.M., Dembelov, M.G., Calais, E., Deverchere, J., 2009. Extension in the Baikal rift: present-day kinematics of passive rifting. Dokl. Earth Sci. 425, 205–209.
Saria, E., Calais, E., Stamps, D.S., Delvaux, D., Hartnady, C.J.H., 2014. Present-day kinematics of the East African rift. J. Geophys. Res. Solid Earth 119, 3584–3600.
Schlische, R.W., 1993. Anatomy and evolution of the Triassic-Jurassic continental rift system, eastern North America. Tectonics 12, 1026–1042.
Sibson, R.H., 1985. A note on fault reactivation. J. Struct. Geol. 7, 751–754.
Sibson, R.H., 2000. Fluid involvement in normal faulting. J. Geodyn. 29, 469–499.
Sigmundsson, F., Einarsson, P., Bilham, R., Sturkell, E., 1995. Rift-transform kinematics in south Iceland: deformation from global positioning system measurements, 1986 to 1992. J. Geophys. Res. Solid Earth 100, 6235–6248.
Simiyu, S.M., Keller, G.R., 2001. An integrated geophysical analysis of the upper crust of the southern Kenya rift. Geophys. J. Int. 147, 543–561.
Smith, M., 1994. Stratigraphic and structural constraints on mechanisms of active rifting in the Gregory Rift, Kenya. Tectonophysics 236, 3–22.
Smith, M., Mosley, P., 1993. Crustal heterogeneity and basement influence on the development of the Kenya Rift, East Africa. Tectonics 12, 591–606.
Spiegel, C., Kohn, B.P., Belton, D.X., Gleadow, A.J.W., 2007. Morphotectonic evolution of the central Kenya rift flanks: implications for late Cenozoic environmental change in East Africa. Geology 35, 427–430.
Stamps, D.S., Calais, E., Saria, E., Hartnady, C., Nocquet, J.-M., Ebinger, C.J., Fernandes, R.M., 2008. A kinematic model for the East African rift. Geophys. Res. Lett. 35. http://dx.doi.org/10.1029/2007GL032781.
Stamps, D.S., Flesch, L.M., Calais, E., Ghosh, A., 2014. Current kinematics and dynamics of Africa and the East African rift system. J. Geophys. Res. Solid Earth 119, 5161–5186.
Strecker, M., Bosworth, W., 1991. Quaternary stress-field change in the Gregory rift, Kenya. EOS Trans. 72, 21–22.
Tibaldi, A., Bonali, F.L., Corazzato, C., 2014. The diverging volcanic rift system. Tectonophysics 611, 94–113.
Vauchez, A., Dineur, F., Rudnick, R., 2005. Microstructure, texture and seismic anisotropy of the lithospheric mantle above a mantle plume: insights from the Labait volcano xenoliths (Tanzania). Earth Planet. Sci. Lett. 232, 295–314.
Versfelt, J., Rosendahl, B.R., 1989. Relationships between pre-rift structure and rift architecture in lakes Tanganyika and Malawi, East Africa. Nature 337, 354–357.
Villamor, P., Berryman, K., 2001. A late Quaternary extension rate in the Taupo Volcanic Zone, New Zealand, derived from fault slip data. N. Z. J. Geol. Geophys. 44, 243–269.
Villamor, P., Berryman, K.R., 2006. Evolution of the southern termination of the Taupo rift, New Zealand. N. Z. J. Geol. Geophys. 49, 23–37.
Walsh, J.J., Watterson, J., 1988. Analysis of the relationship between displacements and dimensions of faults. J. Struct. Geol. 10, 239–247.
Walsh, J.J., Watterson, J., 1991. Geometric and kinematic coherence and scale effects in normal fault systems. Geol. Soc. Spec. Publ. 56, 193–203.
Watkinson, A.J., Ward, E.M.G., 2006. Reactivation of pressure-solution seams by a strike-slip fault-sequential, dilational jog formation and fluid flow. Aapg Bull. 90, 1187–1200.
Wauthier, C., Smets, B., Keir, D., 2015. Diking-induced moderate-magnitude earthquakes on a youthful rift border fault: the 2002 Nyiragongo-Kalehe sequence, DR Congo. Geochem. Geophys. Geosyst. 16, 4280–4291.
Weinstein, A., Oliva, S.J., Ebinger, C.J., Roecker, S., Tiberi, C., Aman, M., Lambert, C., Witkin, E., Albaric, J., Gautier, S., Peyrat, S., et al., 2017. Fault-magma interactions during early continental rifting: seismicity of the Magadi-Natron-Manyara basins, Africa. Geochem. Geophys. Geosyst. http://dx.doi.org/10.1002/2017GC007027.
Wheeler, W.H., Karson, J.A., 1994. Extension and subsidence adjacent to a weak continental transform: an example from the Rukwa Rift, East Africa. Geology 22, 625–628.
Wilkinson, M., Roberts, G.P., McCaffrey, K., Cowie, P.A., Faure Walker, J.P., Papanikolaou, I., Phillips, R.J., Michetti, A.M., Vittori, E., Gregory, L., Wedmore, L., Watson, Z.K., 2015. Slip distributions on active normal faults measured from LiDAR and field mapping of geomorphic offsets: an example from L'Aquila, Italy, and implications for modelling seismic moment release. Geomorphology 237, 130–141.
Willemse, E.J.M., Peacock, D.C.P., Aydin, A., 1997. Nucleation and growth of strike-slip faults in limestones from Somerset, UK. J. Struct. Geol. 19, 1461–1477.
Wilson, C.J.N., Rowland, J.V., 2016. The volcanic, magmatic and tectonic setting of the Taupo Volcanic Zone, New Zealand, reviewed from a geothermal perspective. Geothermics 59, 168–187.
Youash, Y., 1969. Tension tests on layered rocks. Geol. Soc. Am. Bull. 80, 303–306.
Zhang, P.Z., Mao, F.Y., Slemmons, D.B., 1999. Rupture terminations and size of segment boundaries from historical earthquake ruptures in the Basin and Range Province. Tectonophysics 308, 37–52.
Zoback, M.L., 1992. 1st-order and 2nd-order patterns of stress in the lithosphere: the world stress map project. J. Geophys. Res. Solid Earth 97, 11703–11728.